

PLASMA WAVE GENERATION IN THE BEAT-WAVE ACCELERATOR*

ROBERT J. NOBLE

*Stanford Linear Accelerator Center
Stanford University, Stanford, California, 94305*

ABSTRACT

We analytically study the generation of longitudinal plasma waves in an underdense plasma by two electromagnetic waves with frequency difference approximately equal to the plasma frequency, as envisioned in the plasma beat-wave accelerator concept of Tajima and Dawson. The relativistic electron fluid equations describing driven electron oscillations with phase velocities near the speed of light in a cold, collisionless plasma are reduced to a single, approximate ordinary differential equation of a parametrically excited nonlinear oscillator. We give amplitude-phase equations describing the asymptotic solutions to this equation valid for plasma wave amplitudes below wave-breaking. We numerically compare the behavior of the asymptotic equations with that of the original equation and with particle simulation results.

Submitted to *Physical Review A*

* Work supported by the Department of Energy, contract DE - AC03 - 76SF00515.

1. Introduction

Since the original proposal by Tajima and Dawson,¹ the plasma beat-wave accelerator has received much attention as a possible high energy accelerator because of the very high gradients thought to be possible. In this scheme, the electric field of a longitudinal electron plasma oscillation with phase velocity, v_{ph} , near the speed of light, c , accelerates charged particles to high energies. The plasma oscillation is resonantly excited by the ponderomotive force of two collinear beating lasers with frequency difference, $\omega_1 - \omega_2$, approximately equal to the electron plasma frequency, ω_p , in an underdense plasma ($\omega_1, \omega_2 \gg \omega_p$). Gradients of order \sqrt{n} eV/cm are theoretically possible, where n is the electron number density in units of cm^{-3} .

If the transverse dimensions of the beating laser beams are much greater than the induced plasma wavelength, $k_p^{-1} = (k_1 - k_2)^{-1}$, the lasers and plasma wave can be treated approximately as infinite plane waves. Within this approximation Rosenbluth and Liu² analytically studied the growth and saturation of longitudinal plasma waves in a cold, collisionless fluid plasma assuming weak laser strengths ($v_{osc}/c \equiv eE_L/m\omega c \ll 1$) and small amplitude plasma waves ($\Delta n/n \ll 1$ and hence $eE_p/m\omega_p c \ll 1$ if $v_{ph} \simeq c$).

Because the beat-wave generation of plasma waves is a resonant excitation, large amplitude plasma waves may develop even though the lasers are relatively weak. The condition $eE_p/m\omega_p c \ll 1$ can then be violated even though $eE_L/m\omega c \ll 1$. In this paper we analytically study the beat-wave generation of plasma waves with $v_{ph} \simeq c$ in a cold, collisionless fluid plasma subject to the more general condition $eE_p/m\omega_p c \lesssim 1$. In practice particle trapping and wave-breaking occur even if $v_{ph} \simeq c$ in a cold plasma for $eE_p/m\omega_p c \gtrsim 1$, and the fluid

approximation breaks down.³

As a plasma wave is generated by two beating lasers it can scatter laser light up and down in frequency by integer multiples of ω_p (multiple Raman scattering).⁴ The scattered light will also beat, inducing oscillations at various multiples of ω_p . However, for laser frequencies $\omega \gg \omega_p$, this sideband generation is negligible prior to saturation of the plasma wave. For example, when $\omega \simeq 5 - 10\omega_p$, numerical simulation codes indicate that as long as $eE_p/m\omega_p c \lesssim 1$ less than 5% of the relative laser power is scattered into sidebands for times up to saturation of the plasma wave amplitude.⁵

Consequently, to study plasma wave generation and saturation analytically we will neglect the scattered laser sidebands. We then have only two beating electromagnetic plane waves and a plasma wave, all with phase velocities near the speed of light in an underdense plasma. One can then reduce the relativistic plasma fluid equations to an approximate ordinary nonlinear differential equation for the evolution of the longitudinal plasma wave without recourse to the customary linearization procedure. Not surprisingly this equation is equivalent to Poisson's equation with the electron density being modulated by the beating lasers and variations in the plasma wave phase velocity being neglected. The derivation and asymptotic solution of this nonlinear equation are the subject of this paper.

The outline of the paper is as follows. In Section 2 the equations describing nonlinear waves in a relativistic plasma are reviewed to establish notation. In Section 3, starting from the known solution of these equations for a single light wave in an underdense plasma, the approximate ordinary differential equation describing a longitudinal plasma wave driven by two beating light waves is

derived.

Amplitude-phase equations describing the asymptotic solutions of this differential equation are constructed for small amplitude plasma waves ($eE_p/m\omega_p c \ll 1$) in Section 4 and large amplitude waves ($eE_p/m\omega_p c \gtrsim 1$) in Section 5. The numerical solution of these asymptotic equations are compared with that of the original nonlinear differential equation. We find that our small amplitude asymptotic solution agrees with the previous results of Rosenbluth and Liu in the time domain.² For large amplitude waves, our asymptotic solution accurately approximates the numerical solution of the original equation for amplitudes up to $eE_p/m\omega_p c \simeq 1$. Interestingly, our solutions also agree very well with two-dimensional particle simulation results for the temporal evolution of beat-wave generated plasma waves.

We conclude the paper in Section 6 with some comments regarding the experimental implications of our results for plasma wave generation in underdense plasmas.

2. Nonlinear Waves in a Plasma

The equations describing nonlinear waves in a cold, collisionless relativistic plasma with stationary ions have been previously given by Akhiezer et al.⁶ The fluid equations for the electron velocity \bar{v} , electron density n , and the fields \bar{E} and \bar{B} are

$$\begin{aligned} \frac{\partial \bar{p}}{\partial t} + (\bar{v} \cdot \nabla) \bar{p} &= -e\bar{E} - \frac{e}{c}(\bar{v} \times \bar{B}) \\ \nabla \cdot \bar{E} &= 4\pi e(n_0 - n), \quad \nabla \times \bar{E} = -\frac{1}{c} \frac{\partial \bar{B}}{\partial t} \end{aligned} \quad (2.1)$$

$$\nabla \cdot \bar{B} = 0, \quad \nabla \times \bar{B} = -\frac{4\pi}{c} en\bar{v} + \frac{1}{c} \frac{\partial \bar{E}}{\partial t}$$

where \bar{p} is the electron momentum

$$\bar{p} = \frac{m\bar{v}}{\sqrt{1 - v^2/c^2}}, \quad (2.2)$$

and n_0 is the equilibrium electron density.

The wave motion is a function of the single variable $\hat{i} \cdot \bar{r} - v_{ph}t$, where \hat{i} is a unit vector in the direction of propagation, and v_{ph} is the phase velocity. Taking the vector \hat{i} along the z -axis and defining the normalized momentum $\bar{\rho} = \bar{p}/mc$, Akhiezer et al.⁶ obtain from Eqs. (2.1) the following equations for the electron momentum (in the absence of an external magnetic field)

$$\frac{d^2 \rho_x}{d\tau^2} + \frac{\omega_p^2 \beta_{ph}^2}{\beta_{ph}^2 - 1} \frac{\beta_{ph} \rho_x}{\beta_{ph} \sqrt{1 + \rho^2} - \rho_z} = 0 \quad (2.3)$$

$$\frac{d^2 \rho_y}{d\tau^2} + \frac{\omega_p^2 \beta_{ph}^2}{\beta_{ph}^2 - 1} \frac{\beta_{ph} \rho_y}{\beta_{ph} \sqrt{1 + \rho^2} - \rho_z} = 0 \quad (2.4)$$

$$\frac{d^2}{d\tau^2} \left[\beta_{ph} \rho_z - \sqrt{1 + \rho^2} \right] + \frac{\omega_p^2 \beta_{ph}^2 \rho_z}{\beta_{ph} \sqrt{1 + \rho^2} - \rho_z} = 0, \quad (2.5)$$

where

$$\beta_{ph} = \frac{v_{ph}}{c}, \quad \tau = t - \frac{z}{v_{ph}}, \quad \omega_p^2 = \frac{4\pi e^2 n_0}{m}. \quad (2.6)$$

Equations (2.3) - (2.5) describe nonlinear plasma waves, $\bar{\rho}(\tau)$, with a given phase velocity, v_{ph} . Using these equations, the electron density n and the fields \bar{E} and \bar{B} are found from Eqs. (2.1) to be

$$n = \frac{n_0 \beta_{ph}}{\beta_{ph} - u_z} = n_0 \left(1 + \frac{\rho_z}{\beta_{ph} \sqrt{1 + \rho^2} - \rho_z} \right) \quad (2.7)$$

$$E_x = -\frac{mc}{e} \frac{d\rho_x}{d\tau}, \quad B_x = \frac{mc}{e\beta_{ph}} \frac{d\rho_y}{d\tau} \quad (2.8)$$

$$E_y = -\frac{mc}{e} \frac{d\rho_y}{d\tau}, \quad B_y = -\frac{mc}{e\beta_{ph}} \frac{d\rho_x}{d\tau} \quad (2.9)$$

$$E_z = -\frac{mc}{e\beta_{ph}} \frac{d}{d\tau} \left(\beta_{ph} \rho_z - \sqrt{1 + \rho^2} \right), \quad B_z = 0, \quad (2.10)$$

where $u_z = v_z/c$. Hence, once Eqs. (2.3) - (2.5) are solved for the momentum $\bar{\rho}(\tau)$, one can immediately obtain $n(\tau)$, $\bar{E}(\tau)$ and $\bar{B}(\tau)$ for the plasma wave from Eqs. (2.7) - (2.10).

3. Light Waves in a Plasma

3.1 ONE LIGHT WAVE

Equations (2.3) - (2.5) can be used to approximately describe the generation of a longitudinal plasma wave by two light waves in an underdense plasma. The method is suggested by recalling the calculation for a single linearly polarized light wave in an underdense plasma as given by Akhiezer et al.⁶

For a single light wave in an underdense plasma, $\beta_{ph} \simeq 1$, and the electron motion is described by the equations

$$\frac{d^2 \rho_{\perp}}{d\theta^2} + \frac{\rho_{\perp}}{\sqrt{1 + \rho^2} - \rho_z} = 0 \quad (3.1)$$

$$\frac{d^2}{d\theta^2} \left(\rho_z - \sqrt{1 + \rho^2} \right) + \frac{(\beta_{ph}^2 - 1) \rho_z}{\sqrt{1 + \rho^2} - \rho_z} = 0 \quad (3.2)$$

where ρ_{\perp} can be taken as either ρ_x or ρ_y , and

$$\theta = (\beta_{ph}^2 - 1)^{-1/2} \omega_p \tau. \quad (3.3)$$

With $\beta_{ph} \simeq 1$, one concludes from Eq. (3.2) that

$$\sqrt{1 + \rho^2} - \rho_z = \text{constant} > 0. \quad (3.4)$$

Denoting this constant by C^2 , Eq. (3.1) becomes

$$\frac{d^2 \rho_{\perp}}{d\theta^2} + \frac{\rho_{\perp}}{C^2} = 0 \quad (3.5)$$

which has a solution of the form

$$\rho_{\perp} = R_{\perp} \cos \frac{\theta}{C}. \quad (3.6)$$

Since the average of ρ_z over an oscillation vanishes, the constant C^2 is determined from Eqs. (3.4) and (3.6) to be

$$C^2 = \left(1 + \frac{1}{2} R_{\perp}^2\right)^{1/2}. \quad (3.7)$$

The solution for the electron motion is then

$$\rho_{\perp} = R_{\perp} \cos \omega\tau, \quad \rho_z = \frac{R_{\perp}^2 \cos 2\omega\tau}{4\sqrt{1 + \frac{1}{2} R_{\perp}^2}}, \quad (3.8)$$

where

$$\omega = \omega_p (\beta_{ph}^2 - 1)^{-1/2} \left(1 + \frac{1}{2} R_{\perp}^2\right)^{-1/4} \quad (3.9)$$

is the frequency of the light wave.

This is the familiar "Figure 8" motion of a single electron in the field of a plane wave⁷. Since $\omega \gg \omega_p$, low frequency plasma oscillations near ω_p are not

effectively excited, which is the physical content of Eq. (3.4). According to Eq. (2.10) then, $E_z \simeq 0$ in this approximation. Finally note that from Eq. (2.8)

$$E_{\perp}(\tau) = \frac{m\omega c}{e} R_{\perp} \sin \omega \tau , \quad (3.10)$$

so R_{\perp} is the usual quiver velocity parameter " v_{osc}/c " used as a measure of transverse electron motion in a laser field. We see that R_{\perp} is actually a normalized momentum (in units of mc) rather than a velocity.

3.2 TWO LIGHT WAVES

Now let us consider two linearly polarized light waves with frequency difference $\omega_1 - \omega_2 \simeq \omega_p$ in an underdense plasma ($\omega_1, \omega_2 \gg \omega_p$). The beating of these two waves will excite a low frequency longitudinal plasma oscillation. This oscillation and the two light waves have phase velocities near the speed of light. Strictly speaking Eqs. (2.3) - (2.5) are only applicable to a single mode of given phase velocity, but since the phase velocities are nearly equal, we will attempt to treat these three waves in the plasma as approximately a single, coupled longitudinal - transverse mode, $\bar{\rho}(\tau)$. By choosing the initial conditions such that there is no longitudinal motion at, say $\tau = 0$, we would then see longitudinal plasma motion evolve for $\tau > 0$.

Because of the beating between the two light waves, we expect the quantity $\sqrt{1 + \rho^2} - \rho_z$ in Eq. (3.4) to become a slowly varying function of τ rather than a constant as for one light wave. Consequently we define the slow dependent variable

$$x(\tau) = \sqrt{1 + \rho^2} - \rho_z . \quad (3.11)$$

Recall that $dx/d\tau$ is proportional to $E_z(\tau)$, so $x(\tau)$ is proportional to the electric

potential.

Since the phase velocities of the two light waves are nearly the same, we try a solution of the form

$$\rho_{\perp} = \rho_{\perp 1} + \rho_{\perp 2} \quad (3.12)$$

for the transverse motion, where

$$\rho_{\perp 1} = R_{\perp 1} \cos \omega_1 \tau, \quad \rho_{\perp 2} = R_{\perp 2} \cos \omega_2 \tau \quad (3.13)$$

and

$$\begin{aligned} \omega_1 &= \omega + \frac{\Delta\omega}{2} = \omega_p (\beta_1^2 - 1)^{-1/2} x^{-1/2}(\tau) \\ \omega_2 &= \omega - \frac{\Delta\omega}{2} = \omega_p (\beta_2^2 - 1)^{-1/2} x^{-1/2}(\tau). \end{aligned} \quad (3.14)$$

Here $R_{\perp 1,2}$ and $\omega_{1,2}$ are constants, and $\Delta\omega = \omega_1 - \omega_2$. Since $x(\tau)$ implies a longitudinal density modulation, the phase velocities $\beta_{1,2}$ are space-time dependent, although they remain near unity if $\omega_{1,2} \gg \omega_p$. The group velocity $\Delta\omega/\Delta k$ is also approximately c .

The ansatz (3.12) is seen to satisfy Eq. (3.1) in the form

$$\frac{d^2 \rho_{\perp}}{d\tau^2} + \omega^2 \rho_{\perp} = 0 \quad (3.15)$$

to order $\frac{\Delta\omega}{\omega}$, where

$$\omega = \frac{\omega_1 + \omega_2}{2} = \omega_p (\beta^2 - 1)^{-1/2} x^{-1/2}(\tau) \quad (3.16)$$

is a constant, and β is the phase velocity of a light wave with frequency ω . Because $\Delta\omega \ll \omega$, the superposition (3.12) is a very good approximation for the transverse motion. We must still determine an equation for $x(\tau)$ however.

For simplicity we will specialize to the case of equal-intensity lasers, the generalization to different intensities being straightforward. It will be convenient to choose the overall signs of $\rho_{\perp 1}$ and $\rho_{\perp 2}$ such that

$$\rho_{\perp} = R_{\perp}(\cos \omega_1 \tau - \cos \omega_2 \tau) = -2R_{\perp} \sin \omega \tau \sin \frac{\Delta \omega}{2} \tau . \quad (3.17)$$

The corresponding laser electric field is to order $\frac{\Delta \omega}{\omega}$

$$E_{\perp} = \frac{m\omega c}{e} R_{\perp}(\sin \omega_1 \tau - \sin \omega_2 \tau) = \frac{2m\omega c}{e} R_{\perp} \cos \omega \tau \sin \frac{\Delta \omega}{2} \tau . \quad (3.18)$$

Using the solution (3.17) in Eq. (2.5) with $\beta_{ph} = 1$, we obtain an equation for the slow variable $x(\tau)$,

$$\frac{d^2 x}{d(\omega_p \tau)^2} - \frac{1 - x^2 + \rho_{\perp}^2}{2x^2} = 0 , \quad (3.19)$$

where

$$\rho_{\perp}^2 = 4R_{\perp}^2 \sin^2 \omega \tau \sin^2 \frac{\Delta \omega}{2} \tau . \quad (3.20)$$

As long as $\omega \gg \omega_p$, the high frequency part of ρ_{\perp} will not excite oscillations in Eq. (3.19), and $x(\tau)$ will indeed be a slow variable as assumed. We may then replace $\sin^2 \omega \tau$ by its average value of $\frac{1}{2}$, and Eq. (3.19) becomes

$$\frac{d^2 x}{d(\omega_p \tau)^2} - \frac{1 - x^2 + R_{\perp}^2 (1 - \cos \Delta \omega \tau)}{2x^2} = 0 . \quad (3.21)$$

Equation (3.21) describes a parametrically excited nonlinear oscillator (i.e. the excitation appears as a periodic coefficient rather than an inhomogeneous driving term). One can easily show that Eq. (3.21) is equivalent to Poisson's

equation with the electron charge density being modulated by the beating lasers. If $R_{\perp} = 0$, Eq. (3.21) describes free, longitudinal nonlinear plasma oscillations with phase velocity c . Upon solving Eq. (3.21) for $x(\tau)$, one can immediately obtain the longitudinal electron momentum from Eq. (3.11)

$$\rho_z(\tau) = \frac{1 - x^2 + \rho_{\perp}^2}{2x}, \quad (3.22)$$

the electron density from Eq. (2.7)

$$n(\tau) = n_0 \left(1 + \frac{\rho_z}{x}\right), \quad (3.23)$$

and the longitudinal electric field from Eq. (2.10)

$$E_z(\tau) = \frac{mc}{e} \frac{dx}{d\tau}, \quad (3.24)$$

where β_{ph} of the plasma wave is taken as unity.

Because the plasma oscillation frequency is a function of amplitude, the actual phase velocity of the plasma wave, $\omega_p(\text{amplitude}) / (k_1 - k_2)$, will change. Wave-breaking will occur if this phase velocity and the longitudinal electron oscillation velocity approach each other. Equation (3.21) does not exhibit wave-breaking because of the approximation $\beta_{ph} = 1$. However we can estimate from the solution of this equation when wave-breaking would occur simply by comparing the ratio $\omega_p(\text{amplitude})/\Delta\omega$ and the longitudinal electron velocity, v_z/c , assuming $\Delta\omega/\Delta k \simeq c$. The only significant error Eq. (3.21) should make is in underestimating the electron density oscillation which becomes singular at the wave-breaking limit. Eq. (3.21) should be a better approximation for the evolution of the plasma wave in the time domain than in the space domain since the frequency of a free plasma oscillation is independent of the phase velocity (and hence wavelength) in a cold plasma.

4. Small Amplitude Plasma Waves

To study plasma wave generation with Eq. (3.21), we will use the initial conditions

$$x(\tau = 0) = 1, \quad \frac{dx}{d\tau}(\tau = 0) = 0. \quad (4.1)$$

These initial conditions correspond to

$$\rho_z(\tau = 0) = 0, \quad n(\tau = 0) = n_0, \quad E_z(\tau = 0) = 0, \quad (4.2)$$

so there is no longitudinal electron oscillation at $\tau = 0$. We then wish to solve Eq. (3.21) for $\tau > 0$, expecting to see longitudinal motion evolve. The exact analytic solution of Eq. (3.21) is not known, but one can numerically integrate it, as well as construct asymptotic solutions. Both approaches yield insight to the plasma's behavior.

For sufficiently weak lasers ($R_{\perp}^2 \ll 1$), the plasma wave amplitude is small and conventional asymptotic methods can be applied to Eq. (3.21). For small oscillations about $x = 1$ in Eq. (3.21), it is convenient to introduce the variable $y(\tau) = x(\tau) - 1$. Expanding Eq. (3.21) in powers of $y(\tau)$ yields

$$\frac{d^2 y}{d(\omega_p \tau)^2} + y - \frac{3}{2}y^2 + 2y^3 - \frac{5}{2}y^4 + \dots = \frac{1}{2}R_{\perp}^2(1 - \cos \Delta\omega\tau)(1 - 2y + 3y^2 - 4y^3 + \dots), \quad (4.3)$$

with initial conditions $y(\tau = 0) = \frac{dy}{d\tau}(\tau = 0) = 0$. The asymptotic solution of Eq. (4.3) is straightforward using the well-known Krylov - Bogoliubov - Mitropolsky (KBM) method. Since the method is a standard one found in most textbooks on perturbative techniques,⁸ the detailed calculation need not be given here.

We find that the asymptotic solution of Eq. (4.3) uniformly valid for all $\omega_p \tau < O(R_\perp^{-8/3})$ is

$$y(\tau) = a \cos \phi + O(a^2) . \quad (4.4)$$

Here $a(\tau)$ is a slowly varying amplitude, and $\phi(\tau)$ is a rapidly varying phase which satisfy the coupled equations

$$\begin{aligned} \frac{da}{d(\omega_p \tau)} &= -\frac{R_\perp^2}{4} \sin \Phi \\ \frac{d\Phi}{d(\omega_p \tau)} &= \sigma + \frac{3}{16} a^2 + \frac{R_\perp^2}{4} \left(1 - \frac{1}{a} \cos \Phi\right) . \end{aligned} \quad (4.5)$$

In Eqs. (4.5), $\Phi = \Delta\omega\tau - \phi$ is a slowly varying phase, and $\sigma = \frac{\Delta\omega}{\omega_p} - 1$ is the relative frequency mismatch between the laser beat frequency and the plasma frequency. The constant $R_\perp^2/4$ in $d\Phi/d(\omega_p\tau)$ describes the down-shift in the plasma frequency due solely to the lasers (cf. Eq. (3.9)). When this constant is negligible and $\Delta\omega = \omega_p$, Eqs. (4.5) (in the time domain) agree with the amplitude-phase equations of Rosenbluth and Liu² for small amplitude driven plasma waves.

Equations (4.5) can be integrated once to yield

$$\begin{aligned} \left(\frac{da}{d(\omega_p \tau)}\right)^2 &= \left(\frac{R_\perp^2}{4}\right)^2 - \left(\frac{1}{2}\left(\sigma + \frac{R_\perp^2}{4}\right)a + \frac{3}{64}a^3\right)^2 , \\ \frac{R_\perp^2}{4} \cos \Phi &= \frac{1}{2} \left(\sigma + \frac{R_\perp^2}{4}\right) a + \frac{3}{64} a^3 , \end{aligned} \quad (4.6)$$

where we assume $a(\tau = 0) = 0$. Although Eqs. (4.6) can in fact be analytically integrated further to express $a(\tau)$ and $\Phi(\tau)$ in terms of Jacobi elliptic functions, the resulting expressions are so involved for general values of σ and R_\perp^2 as to

yield little insight. It will be sufficient to describe the general behavior of a and Φ .

Initially $a(\tau)$ grows linearly at a rate

$$\frac{da}{d\tau}(\tau = 0) = \frac{1}{4} R_{\perp}^2 \omega_p . \quad (4.7)$$

The amplitude saturates primarily because of mismatch between the driver frequency, $\Delta\omega$, and the free plasma oscillation frequency, ω_o , which decreases with amplitude according to Eq. (4.5),

$$\omega_o = \omega_p \left(1 - \frac{3}{16} a^2\right) . \quad (4.8)$$

Since there is no damping in Eqs. (4.6), the amplitude, a , clearly oscillates in the range $-A \leq a \leq A$, where the saturated amplitude A is a solution of the cubic equation

$$A^3 + \frac{32}{3} \left(\sigma + \frac{R_{\perp}^2}{4}\right) A - \frac{16}{3} R_{\perp}^2 = 0 . \quad (4.9)$$

The frequency - response curve, A as a function of the shifted frequency mismatch, $\sigma + \frac{R_{\perp}^2}{4}$, is sketched in Fig. 1.

When $\sigma = -\frac{R_{\perp}^2}{4}$ (i.e. $\Delta\omega = \left(1 - \frac{1}{4} R_{\perp}^2\right) \omega_p$), the amplitude saturates at

$$a = A_0 \equiv \left(\frac{16}{3} R_{\perp}^2\right)^{1/3} . \quad (4.10)$$

In this case the risetime, τ_r , from $a = 0$ to $a = A_0$ can be easily calculated by integrating Eqs. (4.6),

$$\tau_r\left(\sigma = -\frac{R_{\perp}^2}{4}\right) = \frac{4}{3^{1/4}} K \left(\sqrt{\frac{2 - \sqrt{3}}{4}}\right) \left(\frac{16}{3 R_{\perp}^4}\right)^{1/3} \omega_p^{-1} \simeq 8.5 R_{\perp}^{-4/3} \omega_p^{-1} , \quad (4.11)$$

where $K(k)$ is the complete elliptic integral of the first kind with modulus k .

The frequency - response curve in Fig. 1 exhibits a jump phenomenon when the frequency mismatch $\sigma = (\Delta\omega/\omega_p) - 1$ is near the critical value

$$\sigma^* = - \left(\frac{3}{4} \left(\frac{3R_{\perp}^4}{8} \right)^{1/3} + \frac{R_{\perp}^2}{4} \right). \quad (4.12)$$

For $\sigma \gtrsim \sigma^*$, the amplitude saturates at

$$a = A_+ = 4^{1/3} A_0, \quad (4.13)$$

whereas if $\sigma \lesssim \sigma^*$, saturation occurs at

$$a = A_- = 2^{-1/3} A_0. \quad (4.14)$$

Larger amplitudes can be reached when $\Delta\omega < \omega_p$ because the free plasma oscillation frequency, ω_o , decreases with amplitude, and hence the driver and oscillator are nearer in resonance for finite amplitudes. One finds from the analytic integration of Eqs. (4.6) that the saturation risetime, τ_r , however increases to infinity at σ^* . Beyond this point the mismatch σ is so large that the driver is not strong enough to increase the amplitude sufficiently and reduce ω_o toward $\Delta\omega$. The amplitude then saturates at a lower level just as it does when $\Delta\omega > \omega_p$.

It is straightforward to numerically compare these predictions of the asymptotic solution to the behavior of the exact nonlinear equation (3.21) for the driven plasma oscillation. For our purposes it will be easier to numerically integrate Eqs. (4.5) for a and Φ rather than use the lengthy analytic expressions. We will compare the evolution of the following three quantities: the normalized longitudinal

electric field

$$\frac{eE_z(\tau)}{m\omega_p c} = \frac{dx}{d(\omega_p \tau)}, \quad (4.15)$$

the normalized electron density

$$\frac{n(\tau)}{n_0} = 1 + \frac{d^2 x}{d(\omega_p \tau)^2}, \quad (4.16)$$

and the longitudinal electron velocity

$$u_z(\tau) = \frac{v_z(\tau)}{c} = \frac{n_0}{n(\tau)} \frac{d^2 x}{d(\omega_p \tau)^2}, \quad (4.17)$$

as calculated by numerical integration of the exact equation (3.21) and the asymptotic solution (4.4)-(4.5). With $y(\tau)$ given by Eq. (4.4), the asymptotic expressions for these quantities, valid for all $\omega_p \tau < O(R_\perp^{-8/3})$ are

$$\frac{eE_z(\tau)}{m\omega_p c} = -a \sin \phi + O(a^2), \quad (4.18)$$

$$\frac{n(\tau)}{n_0} = 1 - a \cos \phi + O(a^2), \quad (4.19)$$

$$u_z(\tau) = -a \cos \phi + O(a^2). \quad (4.20)$$

The initial conditions used in the numerical solution of Eqs. (4.5) are $a(\tau = 0) = 0$ and $\Phi(\tau = 0) = -\frac{\pi}{2}$.

Specifically let us consider two interesting examples: (i) $R_\perp = 0.05, \sigma = 0$ and (ii) $R_\perp = 0.05, \sigma \simeq \sigma^*$, corresponding to relatively weak lasers ($R_\perp^2 = 2.5 \times 10^{-3}$). For Case (i), the longitudinal electric field, electron density and electron velocity as calculated numerically from the exact equation (3.21) and asymptotic solution

(4.4) – (4.5) are compared in Figs. 2 - 4. Numerical integration shows that initially $da/d(\omega_p\tau) \simeq 6 \times 10^{-4}$, as predicted by Eq. (4.7), and that the amplitude saturates near $a \simeq 0.23$ when $\tau \simeq 450\omega_p^{-1}$, as would be expected from Eqs. (4.10) and (4.11) since $\sigma = 0 > -R_\perp^2/4$. The oscillation frequency at saturation is approximately $0.99\omega_p$ in Figs. 2-4 for both the exact and asymptotic solutions.

Although the electric field and velocity plots agree reasonably well, the density plots are noticeably different at saturation as evidenced by the density spikes in Fig. 3a. Close inspection of Fig. 2 indicates there is wave-steepening in E_z , which is not reproduced by the asymptotic solution. Since $\nabla \cdot \bar{E} \sim n_0 - n$, such steepening is manifested by spiking of the density oscillation (and to a lesser extent u_z). The lowest order asymptotic expressions contain only single-harmonic trigonometric functions and do not exhibit such wave asymmetries.

In Figs. 5 - 7 similar comparisons of the electric field, electron density and electron velocity are made for Case (ii). According to Eq. (4.12), the critical frequency mismatch should be

$$\sigma^*(R_\perp = 0.05) \simeq -1.06 \times 10^{-2} . \quad (4.21)$$

In Figs. 5 - 7 a value of $\sigma = -9 \times 10^{-3}$ (i.e., $\Delta\omega = 0.991\omega_p$) was used. Since the initial evolution near $\tau = 0$ was essentially the same as in Figs. 2-4, only the behavior near saturation is shown in this case.

As expected from Eq. (4.13), the amplitude does saturate below the value $A_+(R_\perp = 0.05) \simeq 0.38$. At saturation the oscillation frequency is approximately $0.97\omega_p$ for both the exact and asymptotic solutions. The risetime for the asymptotic solution was $\tau_r \simeq 730\omega_p^{-1}$ and increased as σ approached σ^* . The risetime

for the numerical solution of the exact equation (3.21) was $\tau_r \simeq 770\omega_p^{-1}$ at the value of σ used. This difference is probably due to the fact that the actual value of $\sigma^*(R_\perp = 0.05)$ for Eq. (3.21) is approximately -1.04×10^{-2} as determined numerically. In addition Eq. (4.14) was verified numerically when $\sigma \lesssim \sigma^*$ in the exact equation (3.21). Comparison of the density and velocity plots for the exact and asymptotic equations in Figs. 6 and 7 indicates considerable disagreement due to spiking. This is not surprising in that for such large amplitudes we have noticeable wave-steepening in the electric field.

5. Large Amplitude Plasma Waves

Even for relatively weak lasers, large amplitude plasma waves result when driven near resonance. The conventional asymptotic solution (4.4) for the plasma wave does not reproduce the wave-steepening in the electric field and the spiking in the density and velocity oscillations at large amplitudes. One can include higher order harmonics in the solution of Eq. (4.3), but this becomes very laborious for large amplitudes where several terms may be required. For example, the next order asymptotic solution of Eq. (4.3) uniformly valid for all $\omega_p\tau < O(R_\perp^{-2})$ is

$$y(\tau) = a \cos \phi + \frac{a^2}{4} (3 - \cos 2\phi) + O(a^3, R_\perp^2), \quad (5.1)$$

with a and ϕ satisfying Eqs. (4.5). This still does not accurately reproduce wave-steepening, indicating that additional harmonics are needed. Thus one must work harder but loses the simplicity and physical insight provided by a single term asymptotic solution.

Wave-steepening and spiking are well-known characteristics of free, nonlinear plasma oscillations. Equation (3.21) with $R_{\perp} = 0$ describes such free oscillations with phase velocity c ,

$$\frac{d^2 x}{d(\omega_p \tau)^2} - \frac{1 - x^2}{2x^2} = 0, \quad (5.2)$$

and an exact analytic solution is known in terms of the incomplete elliptic integral of the second kind, $E(\psi, k)$.⁹ An obvious improvement on the conventional KBM approximation used earlier is to take this exact nonlinear solution, with a slowly varying amplitude, as the leading term in an asymptotic expansion for the driven plasma wave.

Denoting the argument ψ of $E(\psi, k)$ by E^{-1} , the inverse of the incomplete elliptic integral of the second kind, the solution to Eq. (5.2) can be written as⁹

$$x(\tau) = a - \left(a - \frac{1}{a}\right) \sin^2 \left[E^{-1} \left(\frac{\omega_p \tau}{2a^{1/2}}, k \right) \right] \quad (5.3)$$

(with initial conditions $x(\tau = 0) = a \geq 1$, $\frac{dx}{d\tau}(\tau = 0) = 0$), where

$$k = \left(1 - \frac{1}{a^2}\right)^{1/2}, \quad a = \left(\frac{1 + u_m}{1 - u_m}\right)^{1/2}, \quad (5.4)$$

and u_m is the amplitude of the normalized longitudinal electron velocity, u_z . The free plasma oscillation frequency ($= 2\pi/\text{period}$) is given by

$$\omega_o = \frac{\pi \omega_p}{2a^{1/2} E(k)} = \frac{\pi}{2} \left(\frac{1 - u_m}{1 + u_m}\right)^{1/4} \frac{\omega_p}{E \sqrt{(2u_m/(1 + u_m))}}, \quad (5.5)$$

where $E(k)$ is the complete elliptic integral of the second kind. In Fig. 8, the ratio ω_o/ω_p is shown as a function of u_m . In the nonrelativistic and ultrarelativistic

limits, respectively,

$$\omega_o = \begin{cases} (1 - \frac{3}{16}u_m^2)\omega_p & , \quad u_m \rightarrow 0 \\ \frac{\pi}{2\sqrt{2}}(1 - u_m^2)^{1/4}\omega_p & , \quad u_m \rightarrow 1 . \end{cases} \quad (5.6)$$

If one assumes that the R_{\perp}^2 term in Eq. (3.21) is a weak perturbation of the free oscillator equation (5.2), then the leading term in the asymptotic solution for the driven plasma wave is, from Eq. (5.3),

$$x(\tau) = a - \left(a - \frac{1}{a}\right) \sin^2 \left[E^{-1} \left(\frac{\phi}{2a^{1/2}}, k \right) \right] + O(R_{\perp}^2) , \quad (5.7)$$

where $a(\tau) \geq 1$ is a slowly varying amplitude, and $\phi(\tau)$ is a rapidly varying phase. We can hypothesize the form of the amplitude-phase equations appropriate to Eqs. (5.7) based on the insight gained from our earlier interpretation of the small amplitude equations (4.4) - (4.5). We stress that the following is only a physically plausible conjecture for these equations. Remarkably our intuitive equations provide a very good approximation to the behavior of Eq. (3.21) for all oscillation amplitudes $eE_p/m\omega_p c \lesssim 1$.

Comparing Eqs. (4.8) and (5.6), we replace the perturbative frequency shift $\frac{3}{16}a^2$ in Eqs. (4.5) by the exact nonlinear frequency shift $1 - \frac{\pi}{2a^{1/2}E(k)}$ from Eq. (5.5), and the slowly varying phase becomes $\Phi = \Delta\omega\tau - \frac{\pi}{2a^{1/2}E(k)}\phi$. This insures that when $R_{\perp}^2 = 0$, and hence $da/d(\omega_p\tau) = 0$, we correctly recover the relation $-d\Phi/d(\omega_0\tau) = d\phi/d(\omega_p\tau) = 1$ and the free oscillation solution (5.3). Since R_{\perp}^2 is a weak perturbation, the dependence of the amplitude-phase equations on R_{\perp}^2 need not be determined any better than in the conventional KBM approximation,

with the correspondence in amplitudes being $a(\text{Eq. (4.4)}) = a(\text{Eq. (5.7)}) - 1$. The resulting equations are then

$$\begin{aligned} \frac{da}{d(\omega_p \tau)} &= -\frac{R_{\perp}^2}{4} \sin \Phi \\ \frac{d\Phi}{d(\omega_p \tau)} &= \frac{\Delta\omega}{\omega_p} - \frac{\pi}{2a^{1/2}E(k)} + \frac{R_{\perp}^2}{4} \left(1 - \frac{1}{a-1} \cos \Phi \right). \end{aligned} \quad (5.8)$$

The asymptotic solution (5.7) should be valid for all $\omega_p \tau < O(R_{\perp}^{-10/3})$ if the amplitude and phase are determined by Eqs. (5.8). For small oscillations about $x = 1$, Eqs. (5.7) - (5.8) correctly reduce to Eqs. (4.4) - (4.5).

Although Eqs. (5.8) provide physical insight to the behavior of the driven plasma wave, the presence of the elliptic integral renders these equations intractable to further analytic integration. Consequently in order to compare the behavior of Eqs. (5.7) - (5.8) with that of the exact equation (3.21), we rely on numerical integration of the amplitude-phase equations (5.8) in the following.

Not surprisingly, the solution (5.7) is a much better approximation than the conventional asymptotic solution (4.4) for small amplitude plasma waves. For example, in the case of $R_{\perp} = 0.05$ considered in Section 4, one finds excellent agreement between the numerical solution of Eqs. (3.21) and (5.7) - (5.8). It is more interesting however to compare the exact and asymptotic equations for large amplitude plasma waves where the conventional asymptotic expansion becomes inaccurate.

In particular we will consider an example of relatively strong lasers, with $R_{\perp} = 0.5$. We will again compare the evolution of the longitudinal electric field, electron density and longitudinal electron velocity in Eqs. (4.15) - (4.17) as calculated by numerical integration of Eq. (3.21) and the asymptotic solution

(5.7) - (5.8). The initial conditions used in the numerical integration of Eqs. (5.8) are $a(\tau = 0) = 1, \Phi(\tau = 0) = -\frac{\pi}{2}$.

These quantities are compared in Figs. 9 - 11 when $R_{\perp} = 0.5$ and $\Delta\omega = \omega_p$ (*i.e.*, $\sigma = 0$). Both Eqs. (3.21) and Eqs. (5.7) - (5.8) initially have $da/d(\omega_p\tau) \simeq 0.06$. The electric fields saturate when $\tau \simeq 22\omega_p^{-1}$ at $eE_z/m\omega_p c \simeq 0.81$ for the exact equation (3.21) and $eE_z/m\omega_p c \simeq 0.75$ for the asymptotic equations (5.7) - (5.8). The agreement in all the plots is quite good considering that these are large amplitude oscillations. The longitudinal electron velocity and oscillation frequency at saturation are approximately $0.62c$ and $0.9\omega_p$, respectively, for both the exact and asymptotic solutions.

The case of near-resonant excitation ($\Delta\omega \neq \omega_p$) is also interesting to consider. Numerical investigation of the exact equation (3.21) and the amplitude - phase equations (5.8) at large amplitudes indicates that they exhibit a frequency - response behavior similar to that shown in Fig. 1 for Eqs. (4.5) if one identifies A with the saturated value of $eE_z/m\omega_p c$. The ratios A_{\pm}/A_0 from Eqs. (4.13) and (4.14) continue to hold approximately at large amplitudes for both Eqs. (3.21) and (5.8). However, the value of the critical frequency mismatch, σ^* , for Eqs. (5.8) at a given value of R_{\perp} does differ some from that for Eq. (3.21). For example, when $R_{\perp} = 0.5$, we find that $\sigma^*(Eq. (3.21)) = -0.18$ and $\sigma^*(Eqs. (5.8)) = -0.22$. For large amplitude waves, both Eqs. (3.21) and (5.8) give $E_z(\sigma \gtrsim \sigma^*)/E_z(\sigma = 0) \simeq 2$, whereas for small amplitude waves this ratio is about 1.6.

In Figs. 12 - 14, the electric field, electron density and electron velocity from the numerical solution of Eq. (3.21) and the asymptotic solution (5.7) - (5.8) are compared when $R_{\perp} = 0.5$ and $\Delta\omega = 0.86 \omega_p$ (*i.e.*, $\sigma = -0.14$). The elec-

tric field saturates when $\tau \simeq 45\omega_p^{-1}$ at $eE_z/m\omega_p c \simeq 1.35$ for the exact equation (3.21) and $eE_z/m\omega_p c \simeq 1.25$ for the asymptotic equations (5.7) - (5.8). The plots agree reasonably well with the differences being due primarily to the different values of $\sigma^*(R_\perp = 0.5)$ mentioned above. At saturation the longitudinal electron velocity and oscillation frequency are approximately $0.83c$ and $0.75\omega_p$, respectively, for both the exact and asymptotic solutions. Under these conditions the phase velocity in an actual plasma would have decreased to $0.87c$, which is near wave-breaking.

One can proceed further and compare the asymptotic solution (5.7) to the results of particle simulation codes which numerically solve Maxwell's equations and the equations of motion. We will only make one such comparison here based on the two-dimensional plasma simulation results of Sullivan and Godfrey.⁵ Figs. 15a and 15b are taken from Ref. 5 (with permission of the authors) and show the temporal evolution of two beating laser electric fields,

$$E_\perp = \frac{m\omega c}{e} R_\perp (\sin \omega_1 \tau + \sin \omega_2 \tau); \quad \omega \simeq 10\omega_p, \quad R_\perp = 0.5, \quad \Delta\omega = \omega_p, \quad (5.9)$$

and the resulting longitudinal plasma wave as calculated in a particle simulation. The lasers turn on at $\tau = 25\omega_p^{-1}$ with a risetime we estimate to be $40\omega_p^{-1}$ (*i.e.* $R_\perp(\omega_p \tau) = R_\perp [1 - \exp(-\omega_p \tau / 40)]$; $R_\perp = 0.5$). Figs. 15c and 15d show the longitudinal electric field as calculated from Eq. (3.19) and the asymptotic solution (5.7), respectively, with these laser parameters (and using the appropriate expression for $\rho_\perp(\tau)$ corresponding to $E_\perp(\tau)$ in Eq. (5.9)). The agreement between the plasma simulation and our solutions is excellent. According to our solutions in Figs. 15c and 15d, the longitudinal electric field saturates

near $eE_z/m\omega_p c \simeq 0.65$, while the longitudinal electron velocity and oscillation frequency at saturation are approximately $0.55c$ and $0.94 \omega_p$, respectively.

6. Conclusion

The nonlinear asymptotic solution (5.7) for the driven plasma wave is a very good approximation to the numerical solution of the exact equation (3.21) for times up to saturation and amplitudes up to $eE_p/m\omega_p c \simeq 1$. Wave steepening is correctly accounted for by this solution. Furthermore our solution agrees well with two-dimensional particle simulation results for beat-wave generated plasma waves in the time domain. The occurrence of wave-breaking for a given laser intensity and frequency mismatch can be estimated from our equations by comparing the ratio of the oscillation frequency and laser beat frequency with the longitudinal electron velocity, v_z/c . Our equations indicate that wave-breaking generally occurs for amplitudes near $eE_p/m\omega_p c \simeq 1.3$.

We conclude that our equations, which neglect scattered laser sidebands and variations in the phase velocity, provide an adequate fluid description of the essential physics governing the temporal growth and saturation of large amplitude plasma waves below the wave-breaking limit. According to the amplitude-phase equations, the basic saturation mechanism is frequency mismatch between the laser beat-frequency and the amplitude-dependent plasma frequency as long as particle trapping is small. Since the plasma frequency decreases with amplitude, higher longitudinal gradients can be obtained for a given laser intensity if the laser beat-frequency is less than ω_p by an amount dependent on the laser intensity. The risetime to saturation increases as a result, however. Fig. 16 shows the saturated longitudinal electric field $eE_p/m\omega_p c$ as a function of the laser intensity parameter

R_{\perp}^2 for different values of the relative frequency mismatch σ , as calculated from the numerical solution of Eq. (3.21). The critical frequency mismatch σ^* as a function of R_{\perp}^2 from this same equation is shown in Fig. 17.

The simplicity of our equations facilitates the comparison of different experimental situations. In Table 1 we compare resonant and near-resonant excitation of plasma waves by two equal-intensity beating CO_2 lasers ($\lambda \simeq 10\mu$) in a plasma of density $10^{16} cm^{-3}$ (0.1% of the critical density). The energy absorption by the plasma wave, $E_p^2/2E_{\text{laser}}^2$, is seen to decrease with increasing laser intensity. The advantage of having $\Delta\omega < \omega_p$ is clear with the energy absorption increasing about three times over the case $\Delta\omega = \omega_p$. Indeed, the allowed frequency mismatch in the last row of Table 1 is limited by wave-breaking. At lower laser intensities, where no wave-breaking would occur at the critical frequency mismatch, the energy absorption would be about four times the case $\Delta\omega = \omega_p$. The calculated energy absorption percentages in Table 1 are for $\omega \simeq 33\omega_p$ and vary like ω^{-2} for different ω .

ACKNOWLEDGEMENTS

The author would like to thank W. Spence and S. Yu for useful discussions and H. Shoae for aid with various numerical analysis problems during the course of this work.

REFERENCES

1. T. Tajima and J. M. Dawson, Phys. Rev. Lett. 43, 267 (1979). T. Tajima, IEEE Trans. Nucl. Sci. NS-28, 3416 (1981).
2. M. N. Rosenbluth and C. S. Liu, Phys. Rev. Lett. 29, 701 (1972).
3. J. M. Dawson and R. Shanny, Phys. Fluids 11, 1506 (1968). R. D. Ruth and A. W. Chao, Laser Acceleration of Particles (Los Alamos, 1982), P. J. Channel, ed. (A.I.P. Conf. Proc. No. 91, Amer. Inst. of Physics, New York, 1982) p.94.
4. D. Eimerl, R. S. Hargrove and J. A. Pasiner, Phys. Rev. Lett. 46, 651 (1981). C. Joshi, T. Tajima, J. M. Dawson, H. A. Baldis and N. A. Ebrahim, Phys. Rev. Lett. 47, 1285 (1981).
5. D. J. Sullivan and B. B. Godfrey, Laser Acceleration of Particles, (Los Alamos, 1982), *ibid.*, p. 43; The Challenge of Ultra-High Energies, J. Mulvey, ed. (ECFA 83/68, RAL, Oxford, 1983), p.209.
6. A. I. Akhiezer and R. V. Polovin, Sov. Phys. JETP 3, 696 (1956). A. I. Akhiezer, I. A. Akhiezer, R. V. Polovin, A. G. Sitenko and K. N. Stepanov, Plasma Electrodynamics, Vol. 2 (Pergamon, New York, 1975).
7. L. D. Landau and E. M. Lifshitz, The Classical Theory of Fields, Course of Theoretical Physics, Vol. 2, 4th Edition (Pergamon, New York, 1975), p.118.
8. A. H. Nayfeh, Introduction to Perturbation Techniques (Wiley, New York, 1981). For the benefit of the reader unfamiliar with this technique, we note that the KBM method applied to Eq. (4.3) seeks a uniform expansion (i.e. no secular or small divisor terms) for the solution as a series $y(\tau) =$

$\epsilon a \cos \phi + \epsilon^2 y_2(a, \phi) + \dots$, where ϵ is a perturbative bookkeeping device set to unity at the end of the calculation. The amplitude-phase equations are series of the form $da/d(\omega_p \tau) = \epsilon A_1(a) + \epsilon^2 A_2(a) + \dots$ and $d\phi/d(\omega_p \tau) = 1 + \epsilon \Phi_1(a) + \epsilon^2 \Phi_2(a) + \dots$. Using these expansions in Eq. (4.3) and solving for the y_n, A_n and Φ_n order by order in ϵ , one finds that the scaling $R_{\perp}^2 \equiv \epsilon^3 f$ insures uniform behavior of the series $y(\tau)$. The amplitude-phase equations (4.5) have relegated secular terms to $\mathcal{O}(\epsilon^5 \omega_p \tau)$, involving terms proportional to $a^5 \omega_p \tau$ and $a^2 R_{\perp}^2 \omega_p \tau$. Consequently the solution (4.4) is uniformly valid for all $\omega_p \tau < \mathcal{O}(\epsilon^{-4})$, which we designate by the symbolic notation $\mathcal{O}(R_{\perp}^{-8/3})$.

9. R. J. Noble, Proc. of the 12th Int'l. Conf. on High-Energy Accelerators (Fermilab, August 11-16, 1983), F. T. Cole and R. Donaldson, eds. (FNAL, Batavia, 1983), p. 467.

Table 1

Comparison of resonant and near-resonant excitation of plasma waves by two equal-intensity beating CO_2 lasers ($\lambda_1 = 10.6\mu$, $\lambda_2 = 10.3\mu$, $\omega/\omega_p \simeq 33$, $n_0 \simeq 10^{16}cm^{-3}$) based on the analysis of Sections 4 and 5. The gradient in the last row is limited by wave-breaking. The laser quiver velocity is v_{osc}/c . The ratio of the laser beat frequency and plasma frequency is $\Delta\omega/\omega_p$. The combined laser intensity is $I = 2 \times cE_{laser}^2/8\pi$ in units of $watts/cm^2$.

$\frac{v_{osc}}{c}$	$\frac{\Delta\omega}{\omega_p}$	$I(W/cm^2)$	$\frac{eE_p}{m\omega_p c}$	Gradient (GeV/m)	Energy Absorption
0.05	1	7×10^{13}	0.23	2.3	1%
0.05	0.99	7×10^{13}	0.38	3.8	3%
0.5	1	7×10^{15}	0.8	8.0	0.1%
0.5	0.86	7×10^{15}	1.3	13	0.3%

FIGURE CAPTIONS

Fig. 1 Frequency-response curve, A as a function of the shifted frequency mismatch $\sigma + R_{\perp}^2/4$, in Eq. (4.9). The frequency σ^* is given by Eq. (4.12), and the amplitudes A_0 , A_+ and A_- are defined by Eqs. (4.10), (4.13) and (4.14), respectively. The upper dashed curve represents amplitudes obtained by adiabatically decreasing the frequency mismatch, while the lower dashed curve represents unstable amplitudes.

Fig. 2 Longitudinal electric field as a function of $\omega_p\tau$ calculated from (a) the exact equation (3.21) and (b) the asymptotic solution (4.4) - (4.5) for the case $R_{\perp} = 0.05$, $\Delta\omega = \omega_p$.

Fig. 3 Electron density as a function of $\omega_p\tau$ calculated from (a) the exact equation (3.21) and (b) the asymptotic solution (4.4) - (4.5) for the case $R_{\perp} = 0.05$, $\Delta\omega = \omega_p$.

Fig. 4 Longitudinal electron velocity as function of $\omega_p\tau$ calculated from (a) the exact equation (3.21) and (b) the asymptotic solution (4.4) - (4.5) for the case $R_{\perp} = 0.05$, $\Delta\omega = \omega_p$.

Fig. 5 Longitudinal electric field as a function of $\omega_p\tau$ calculated from (a) the exact equation (3.21) and (b) the asymptotic solution (4.4) - (4.5) for the case $R_{\perp} = 0.05$, $\Delta\omega = 0.991\omega_p$.

Fig. 6 Electron density as a function of $\omega_p\tau$ calculated from (a) the exact equation (3.21) and (b) the asymptotic solution (4.4) - (4.5) for the case $R_{\perp} = 0.05$, $\Delta\omega = 0.991\omega_p$.

Fig. 7 Longitudinal electron velocity as a function of $\omega_p\tau$ calculated from (a) the exact equation (3.21) and (b) the asymptotic solution (4.4) - (4.5)

for the case $R_{\perp} = 0.05$, $\Delta\omega = 0.991\omega_p$.

Fig. 8 Free plasma oscillation frequency ratio ω_o/ω_p as a function of the longitudinal electron velocity amplitude u_m .

Fig. 9 Longitudinal electric field as a function of $\omega_p\tau$ calculated from (a) the exact equation (3.21) and (b) the asymptotic solution (5.7) - (5.8) for the case $R_{\perp} = 0.5$, $\Delta\omega = \omega_p$.

Fig. 10 Electron density as a function of $\omega_p\tau$ calculated from (a) the exact equation (3.21) and (b) the asymptotic solution (5.7) - (5.8) for the case $R_{\perp} = 0.5$, $\Delta\omega = \omega_p$.

Fig. 11 Longitudinal electron velocity as a function of $\omega_p\tau$ calculated from (a) the exact equation (3.21) and (b) the asymptotic solution (5.7) - (5.8) for the case $R_{\perp} = 0.5$, $\Delta\omega = \omega_p$.

Fig. 12 Longitudinal electric field as a function of $\omega_p\tau$ calculated from (a) the exact equation (3.21) and (b) the asymptotic solution (5.7) - (5.8) for the case $R_{\perp} = 0.5$, $\Delta\omega = 0.86\omega_p$.

Fig. 13 Electron density as a function of $\omega_p\tau$ calculated from (a) the exact equation (3.21) and (b) the asymptotic solution (5.7) - (5.8) for the case $R_{\perp} = 0.5$, $\Delta\omega = 0.86\omega_p$.

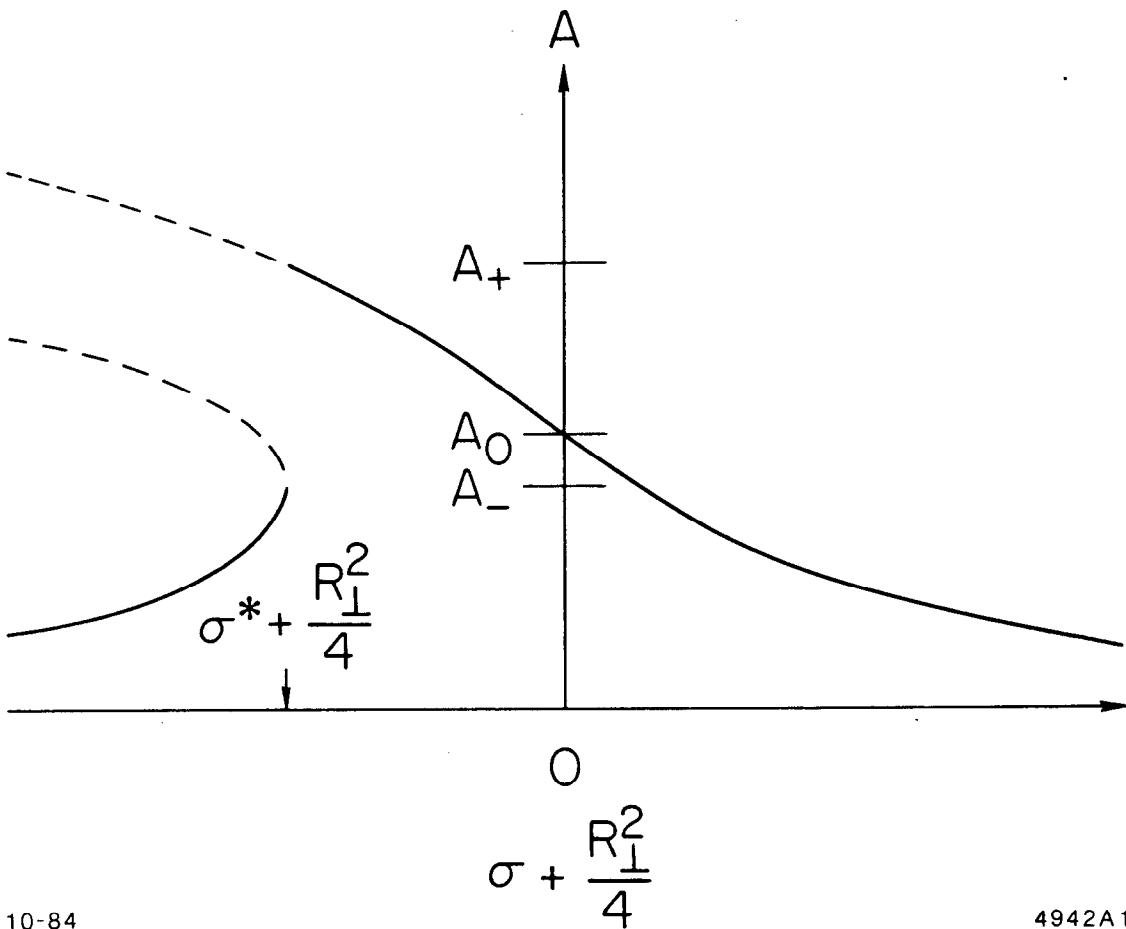
Fig 14 Longitudinal electron velocity as a function of $\omega_p\tau$ calculated from (a) the exact equation (3.21) and (b) the asymptotic solution (5.7) - (5.8) for the case $R_{\perp} = 0.5$, $\Delta\omega = 0.86\omega_p$.

Fig. 15 Temporal evolution of (a) two beating laser electric fields ($\omega_1 = 10.6\omega_p, \omega_2 = 9.6\omega_p, R_{\perp} = 0.5$) and (b) the resulting longitudinal plasma electric field as calculated in a particle simulation (taken from Ref. 5 with

permission of the authors). For comparison the longitudinal plasma electric field as calculated numerically from (c) the exact equation (3.19) and (d) the asymptotic solution (5.7) with the same laser parameters are also shown.

Fig. 16 Saturated longitudinal electric field $eE_p/m\omega_p c$ as a function of the laser intensity parameter R_\perp^2 when the relative frequency mismatch $\sigma = \sigma^*, -R_\perp^2/4$ and 0, as calculated from the numerical solution of Eq. (3.21). The critical frequency mismatch is denoted by σ^* .

Fig. 17 The negative of the critical frequency mismatch σ^* as a function of the laser intensity parameter R_\perp^2 from the numerical solution of Eq. (3.21).



10-84

4942A1

Fig. 1

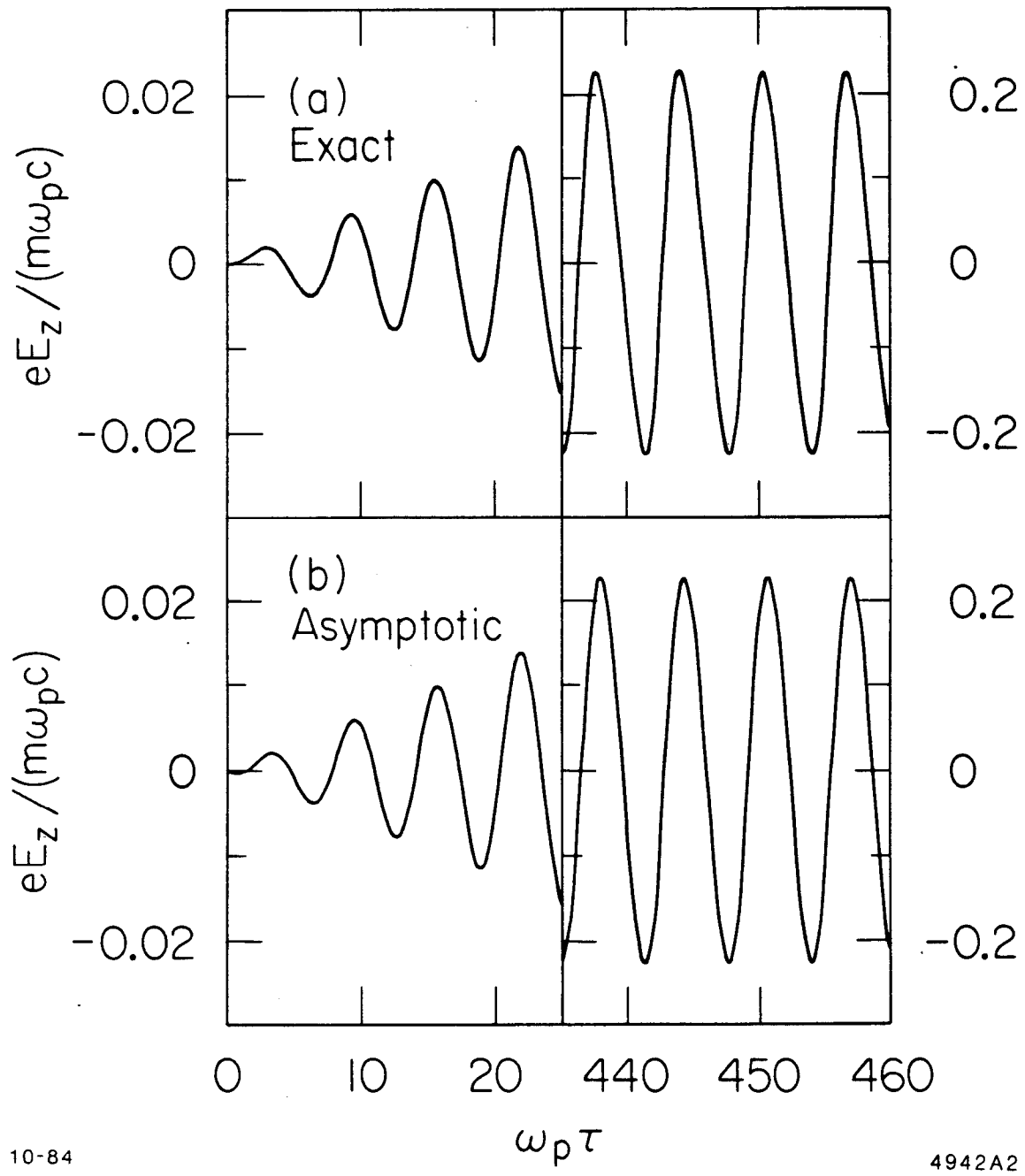


Fig. 2

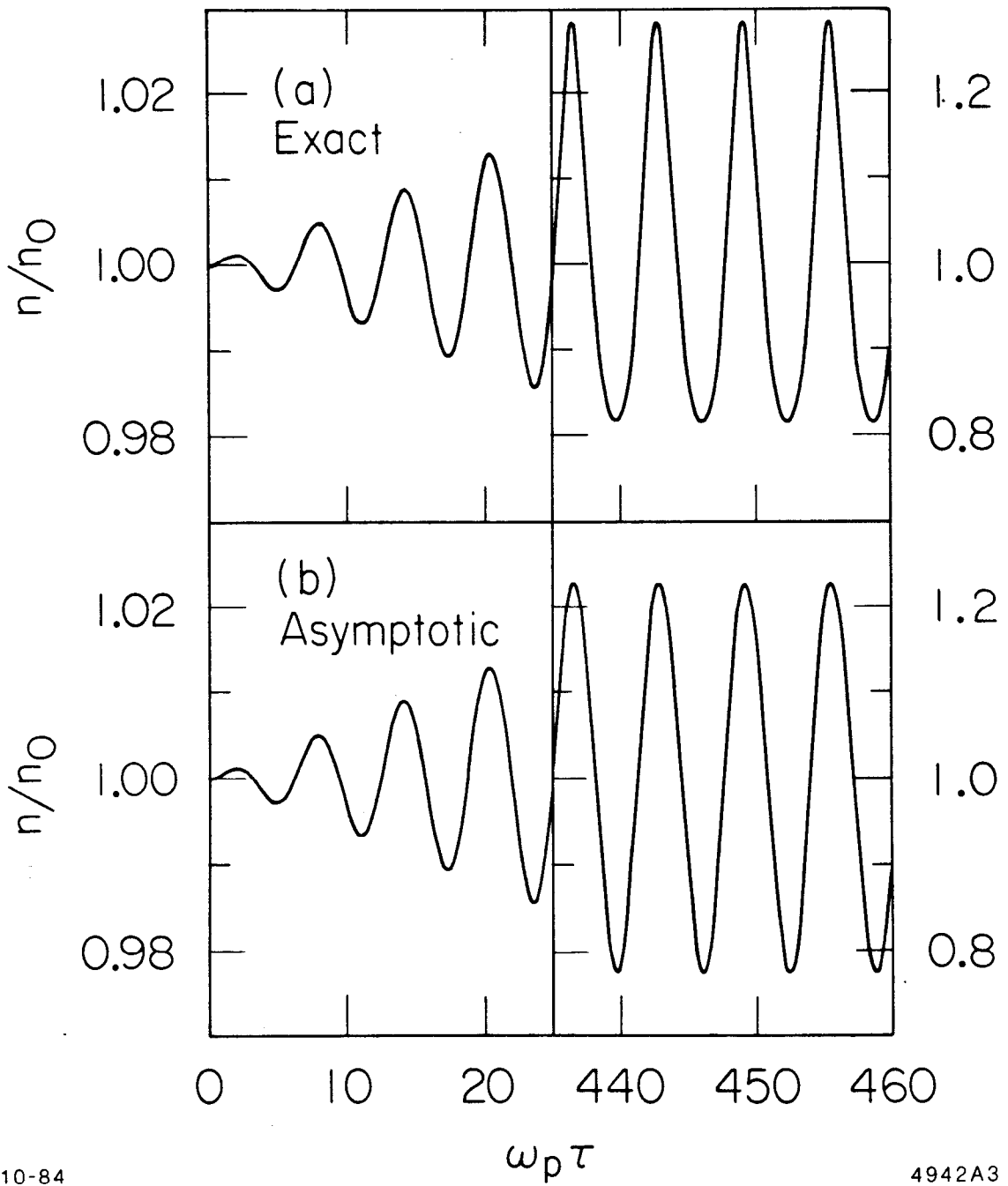
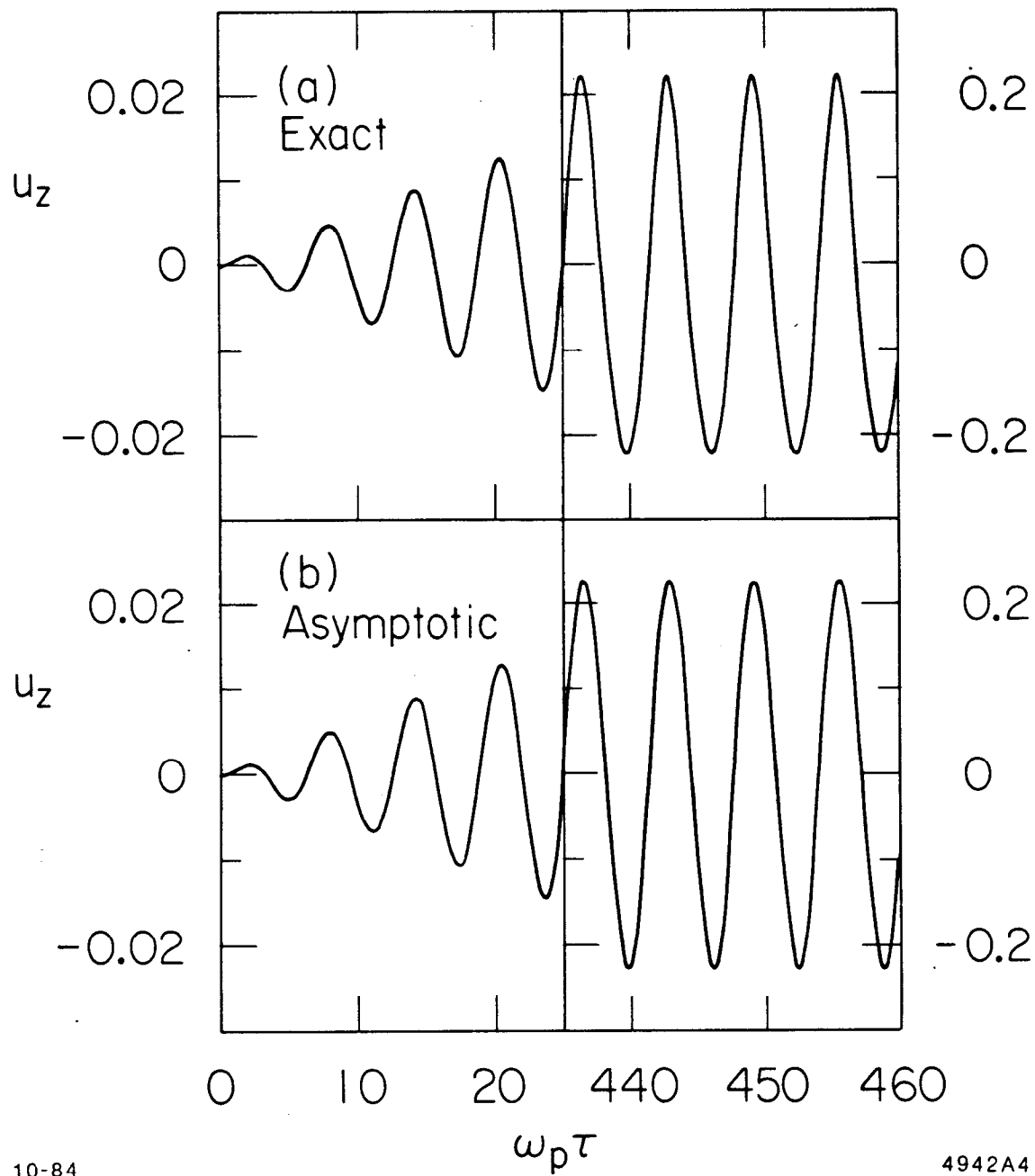


Fig. 3



10-84

4942A4

Fig. 4

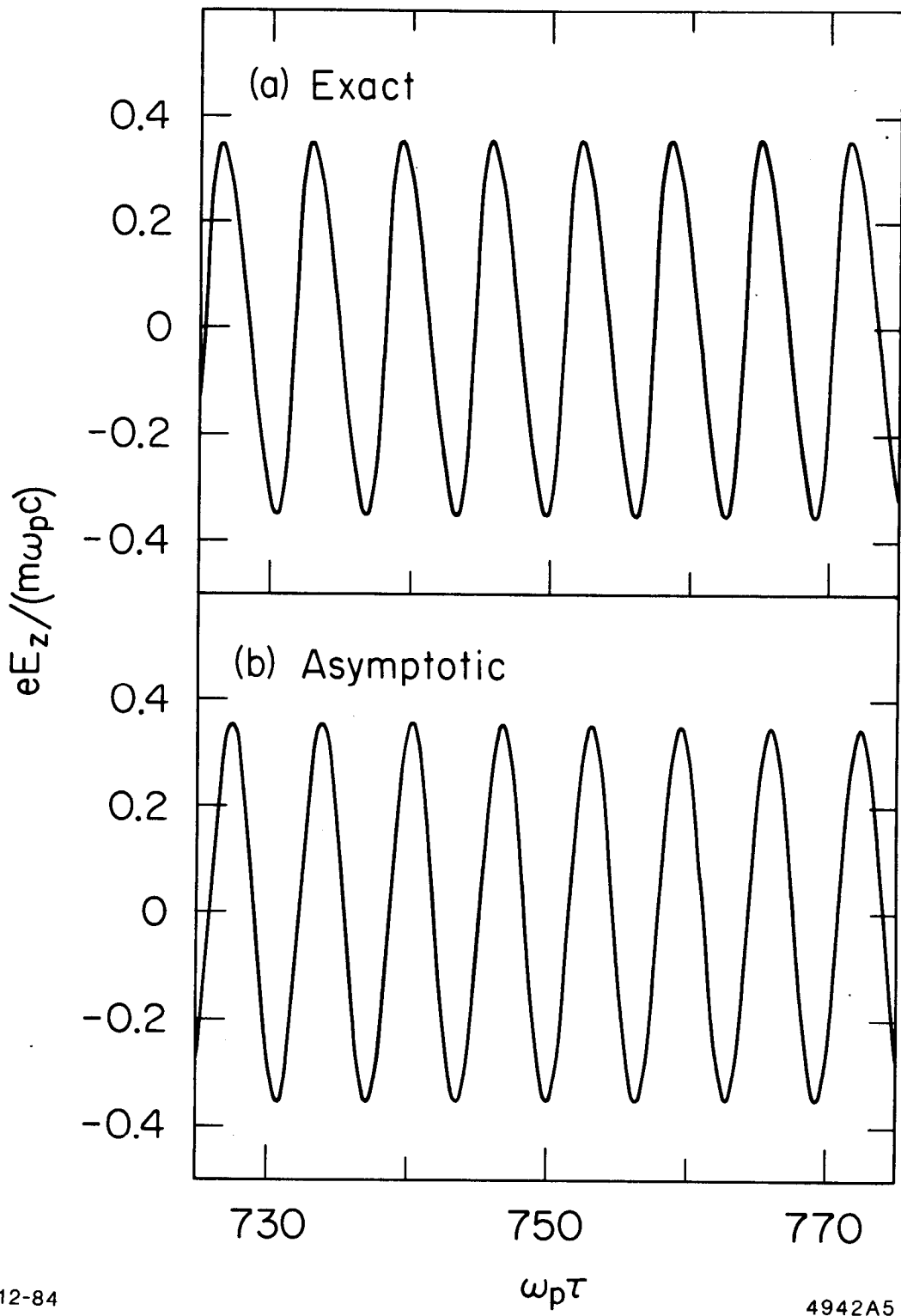


Fig. 5

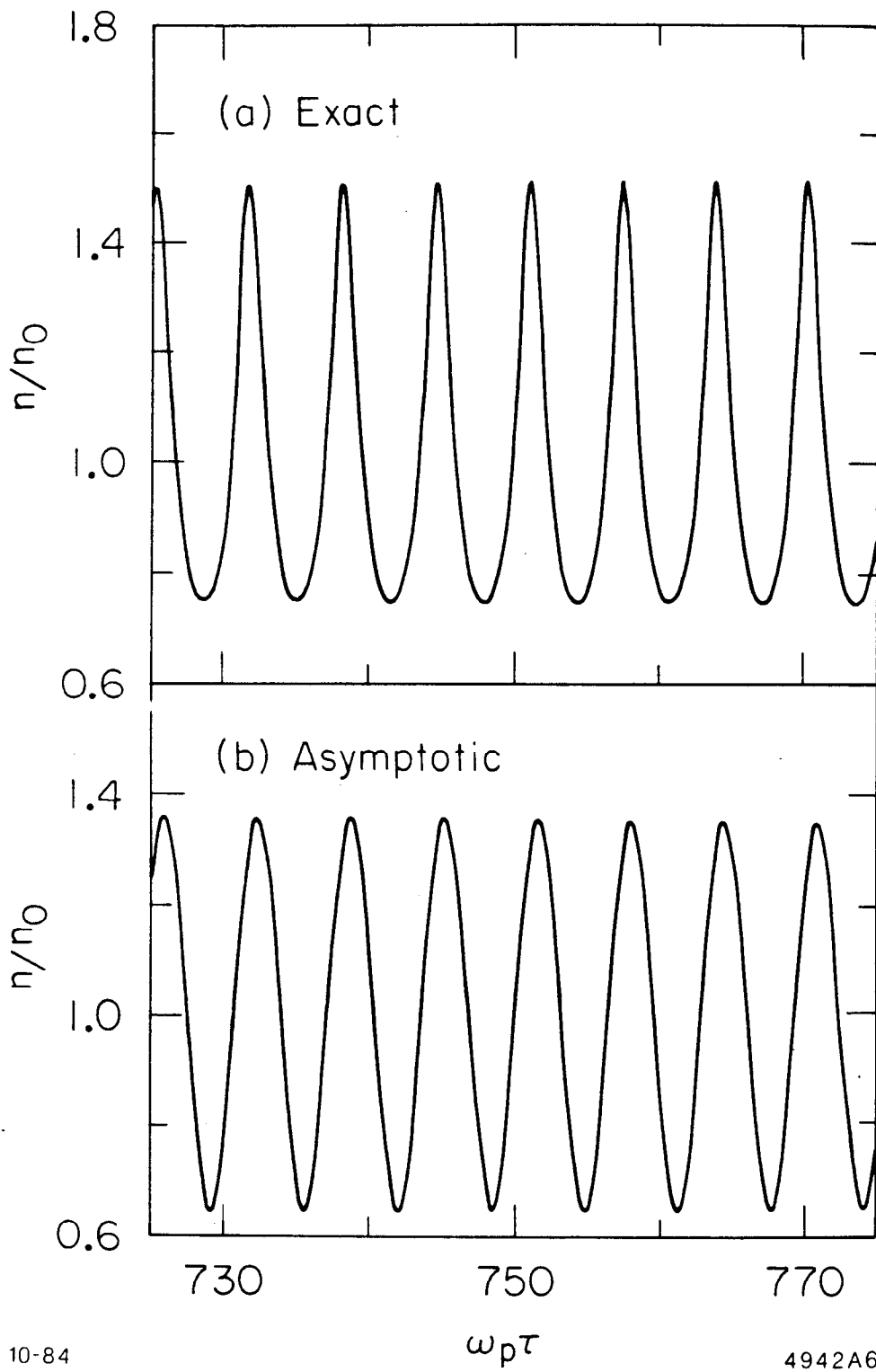


Fig. 6

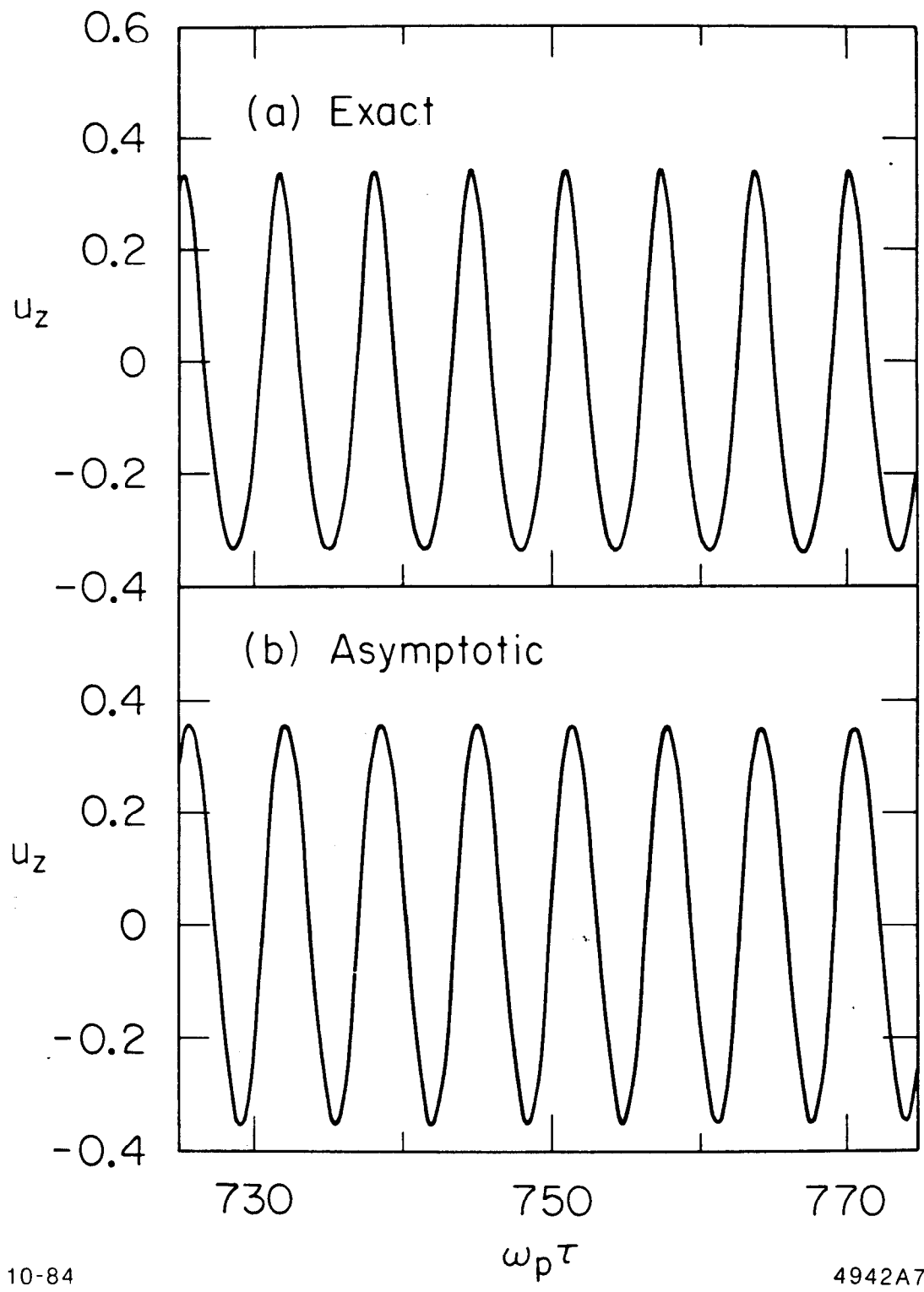


Fig. 7

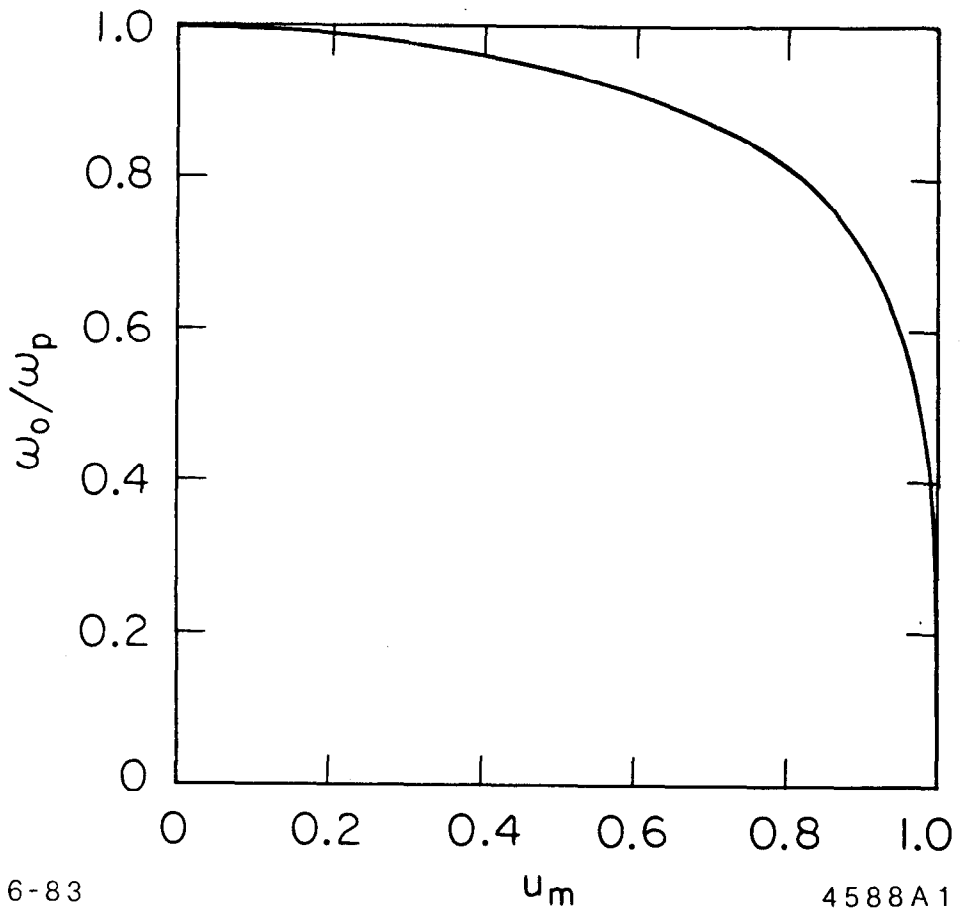


Fig. 8

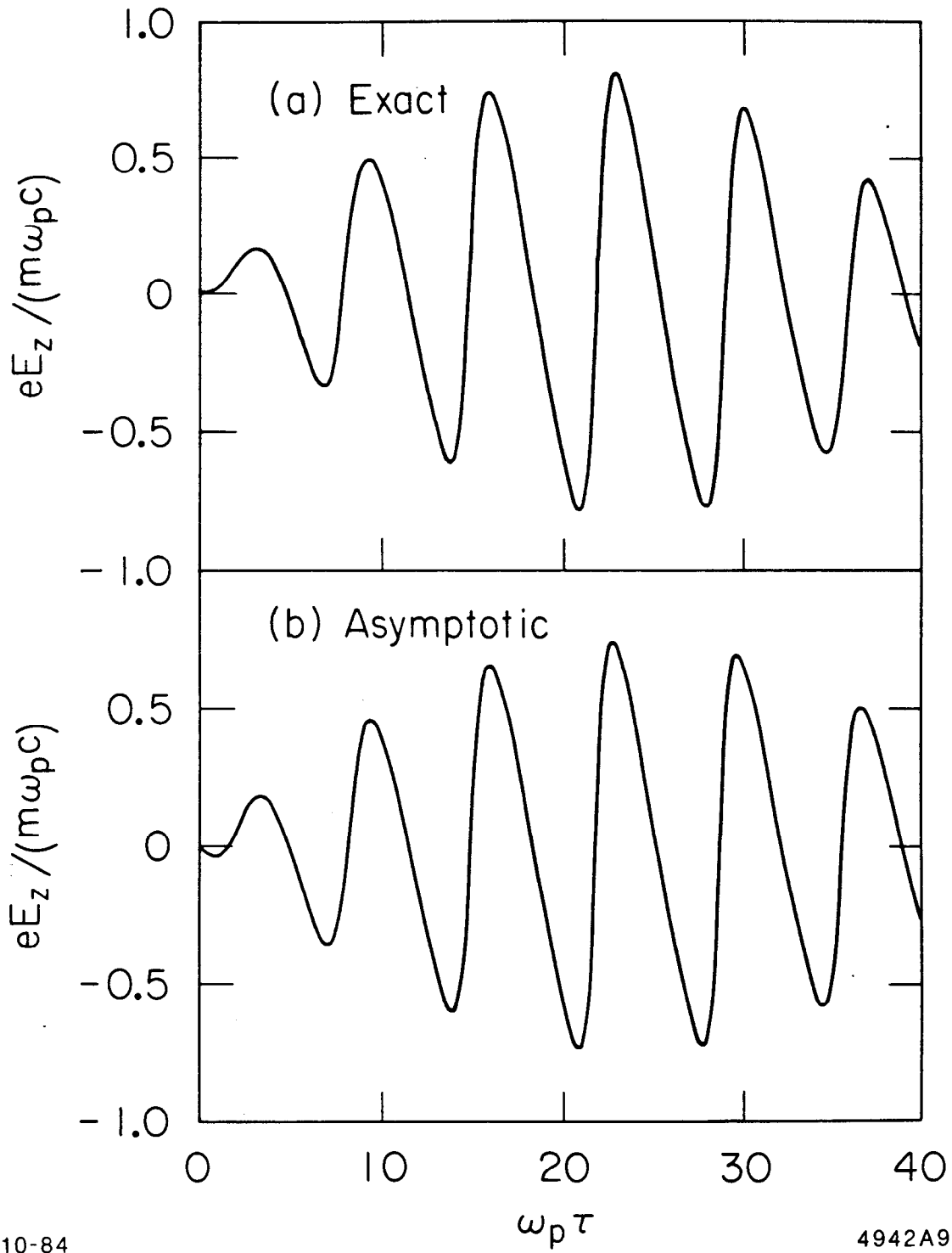
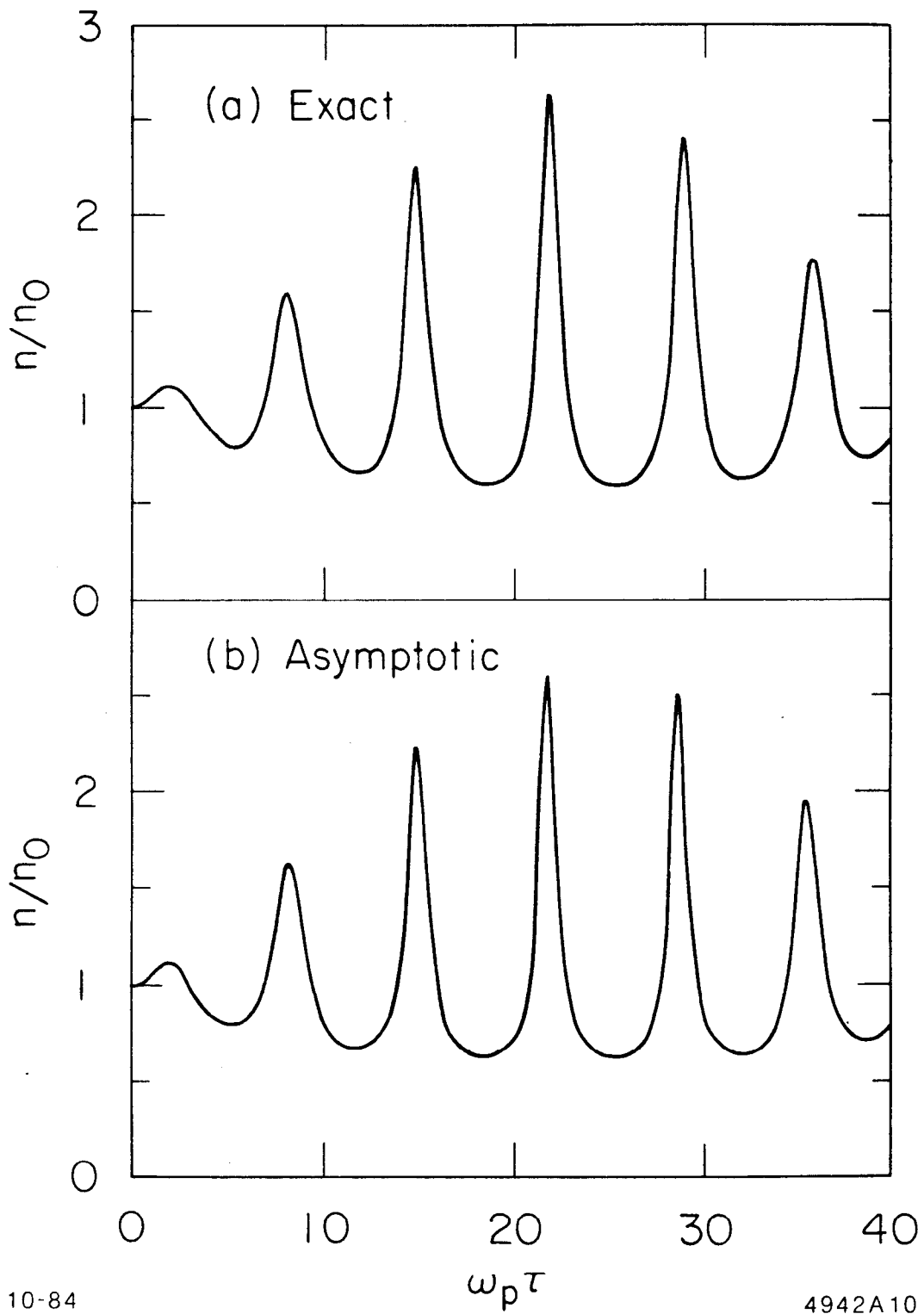


Fig. 9



10-84

$\omega_p \tau$

4942A10

Fig. 10

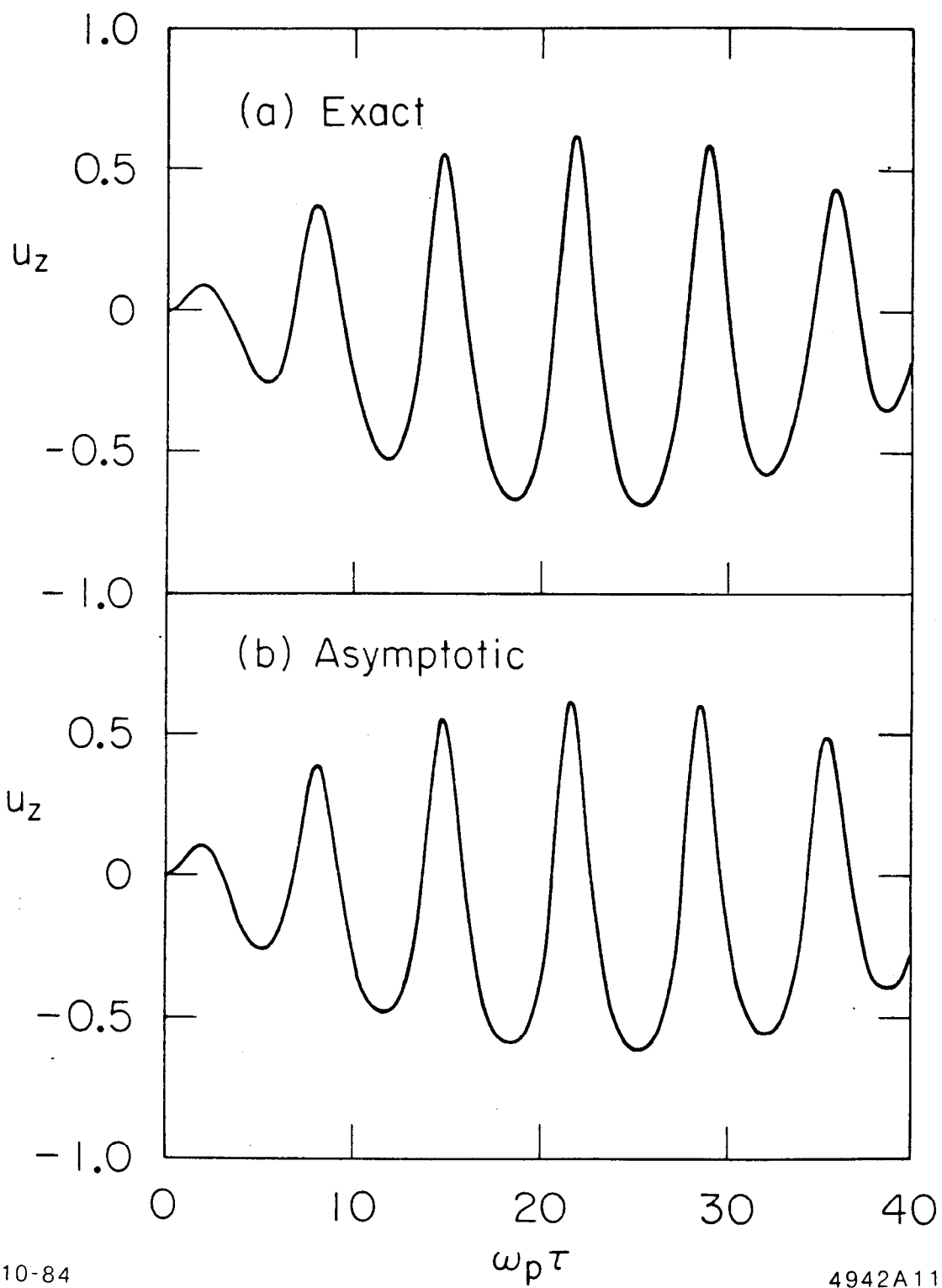


Fig. 11

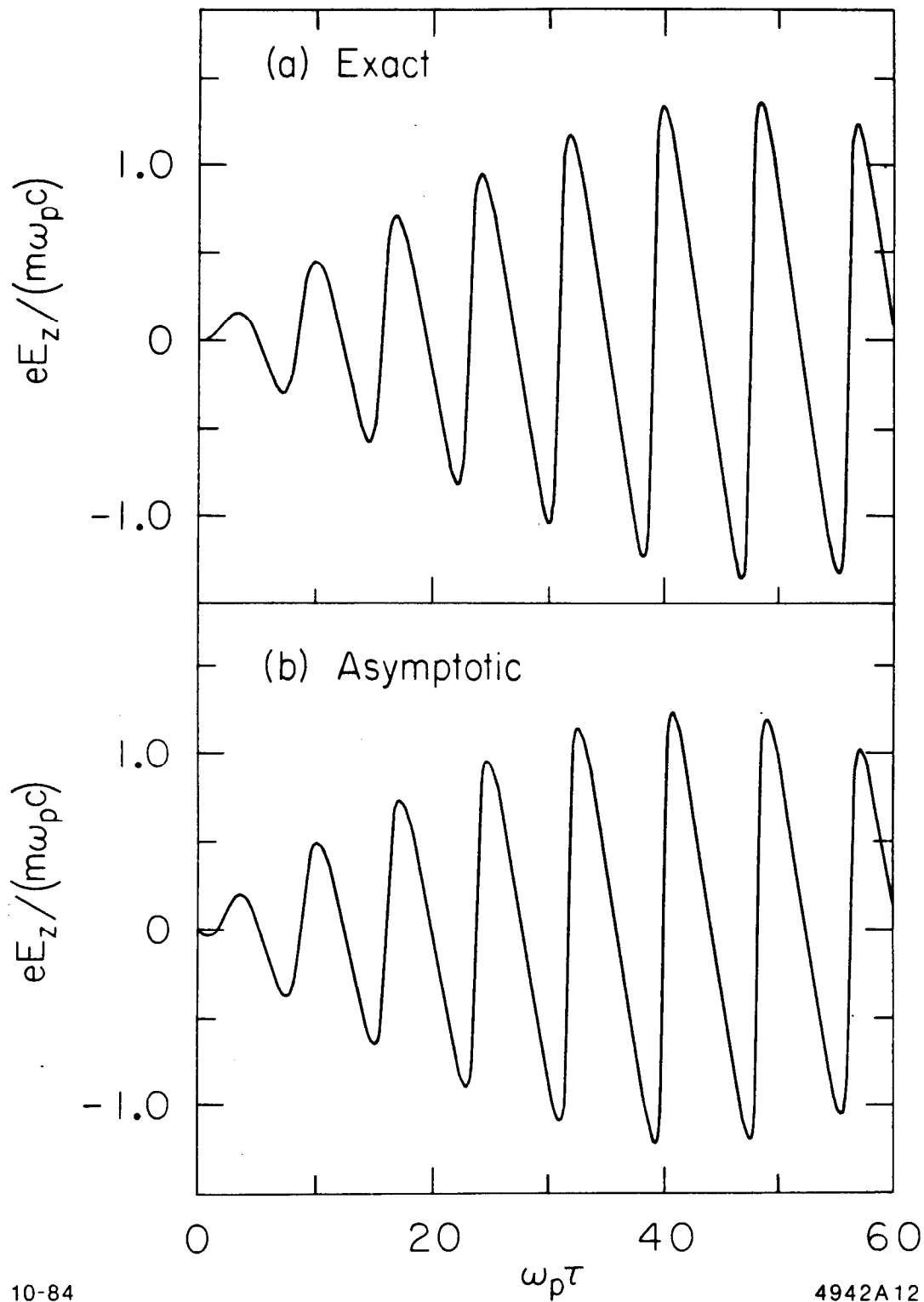


Fig. 12

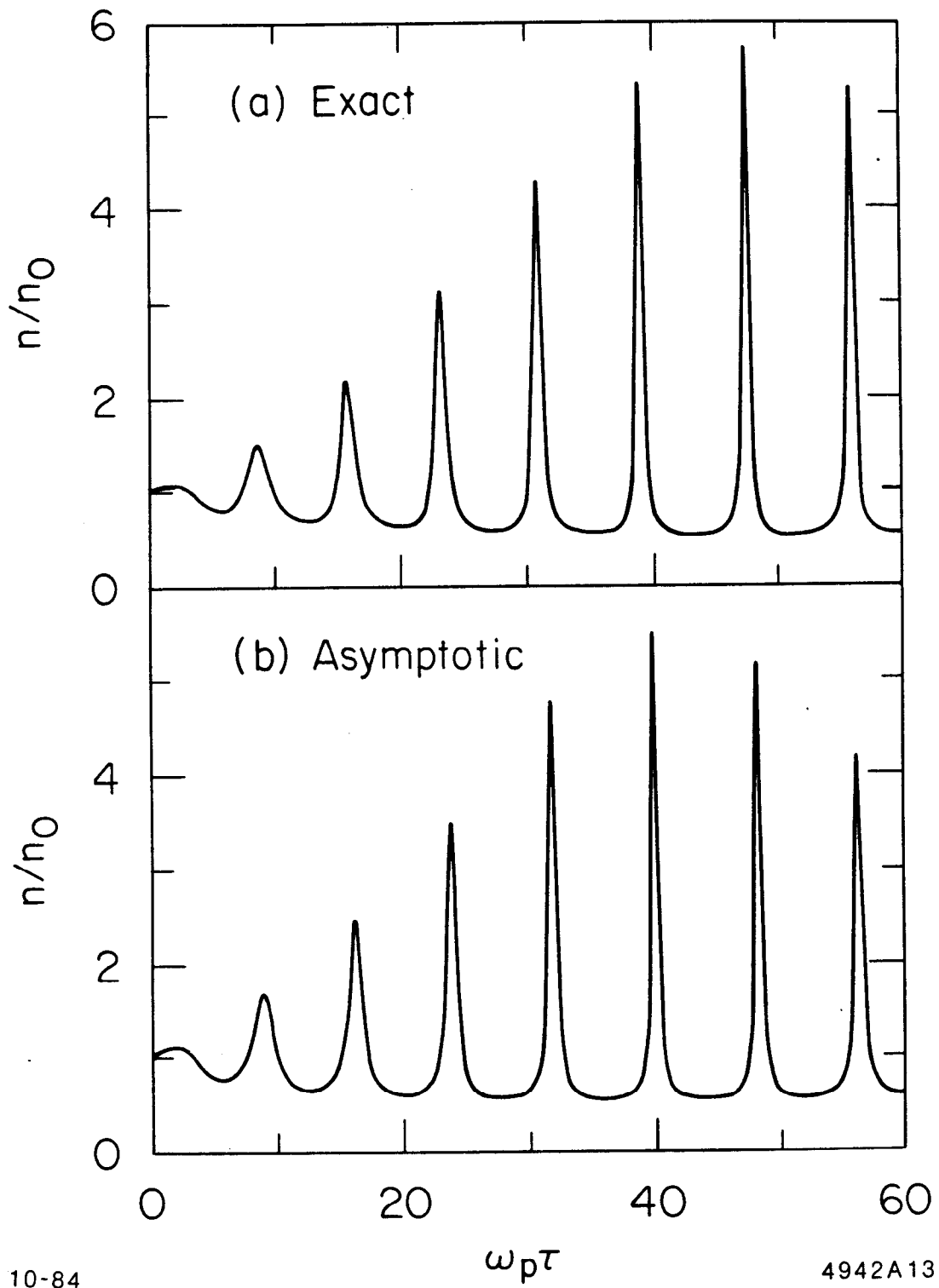


Fig. 13

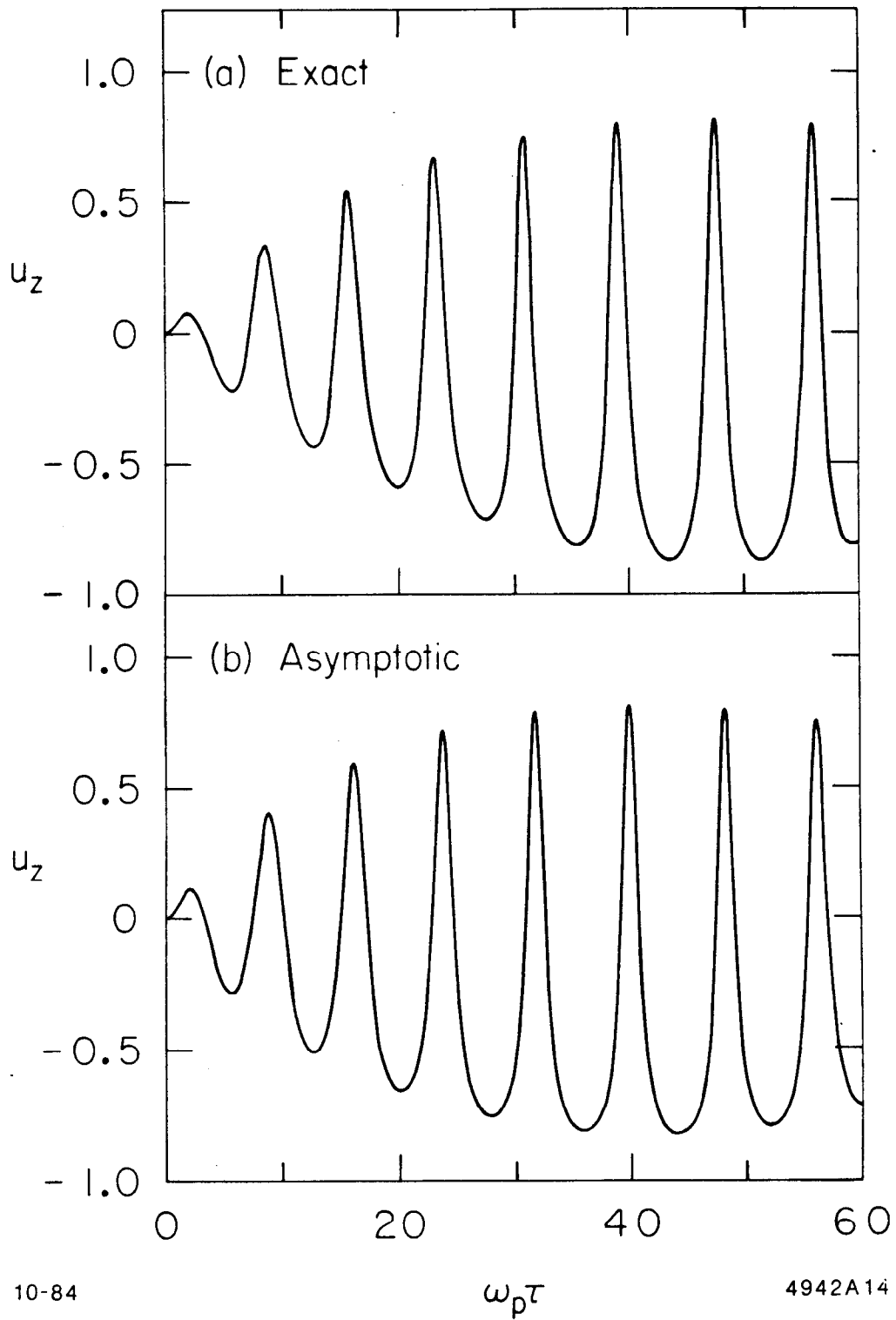


Fig. 14

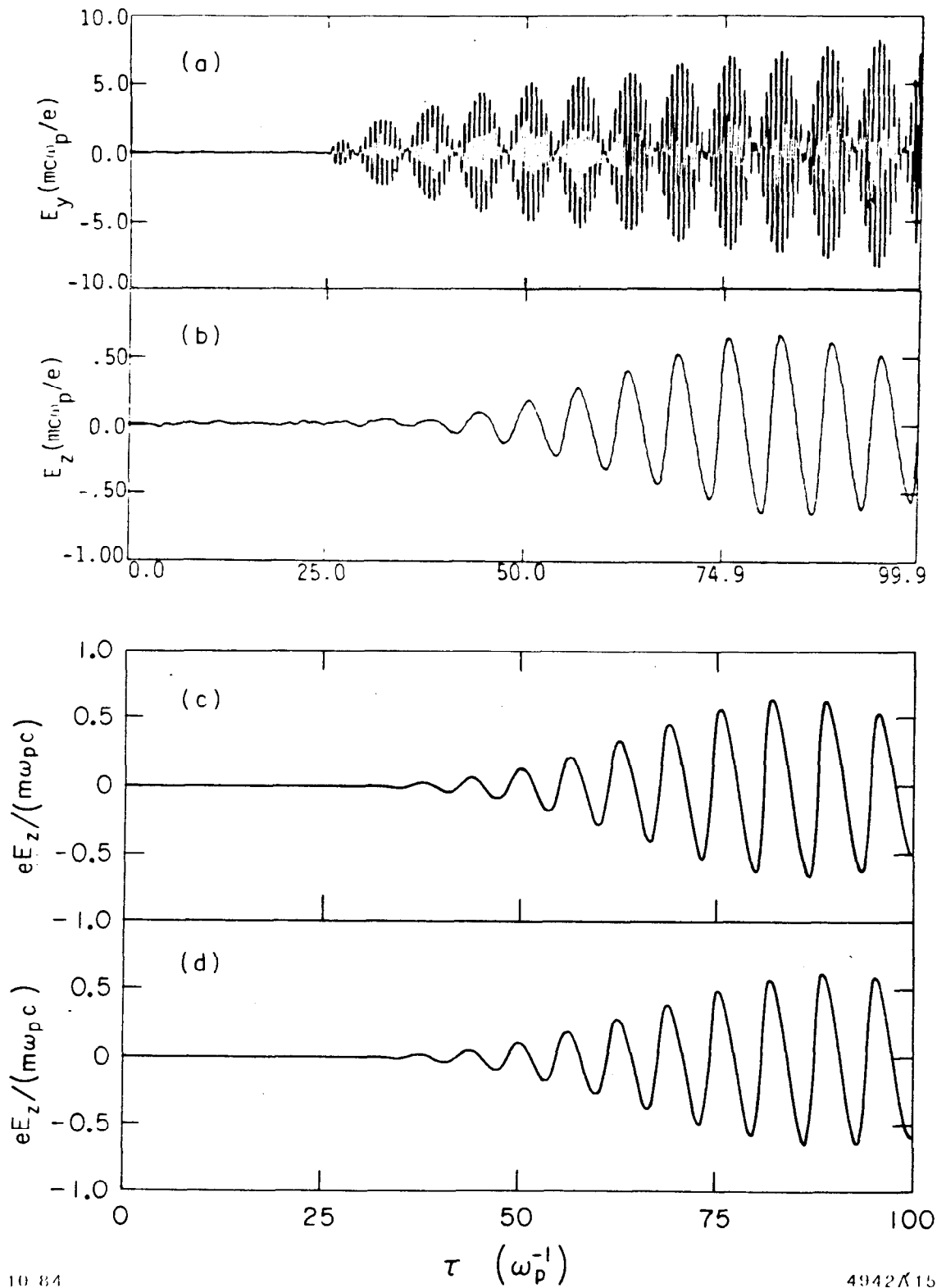
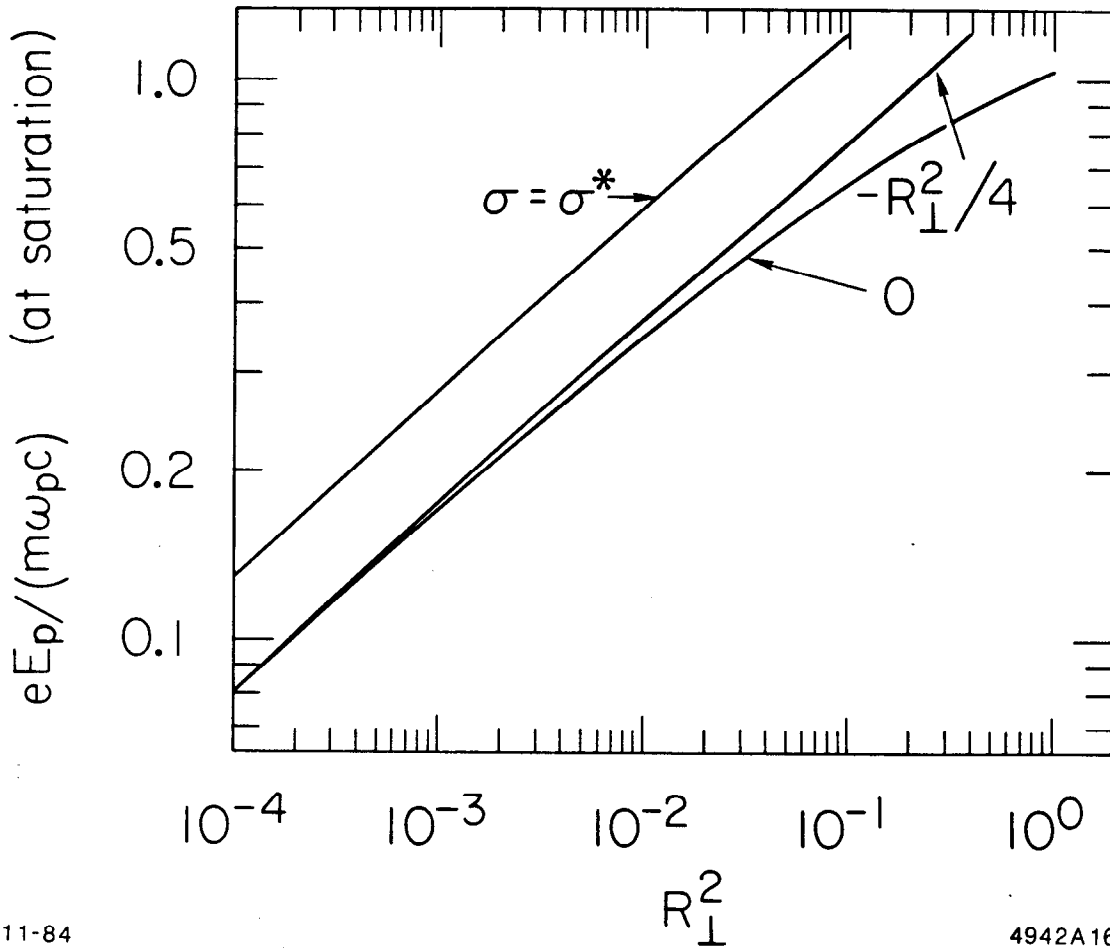


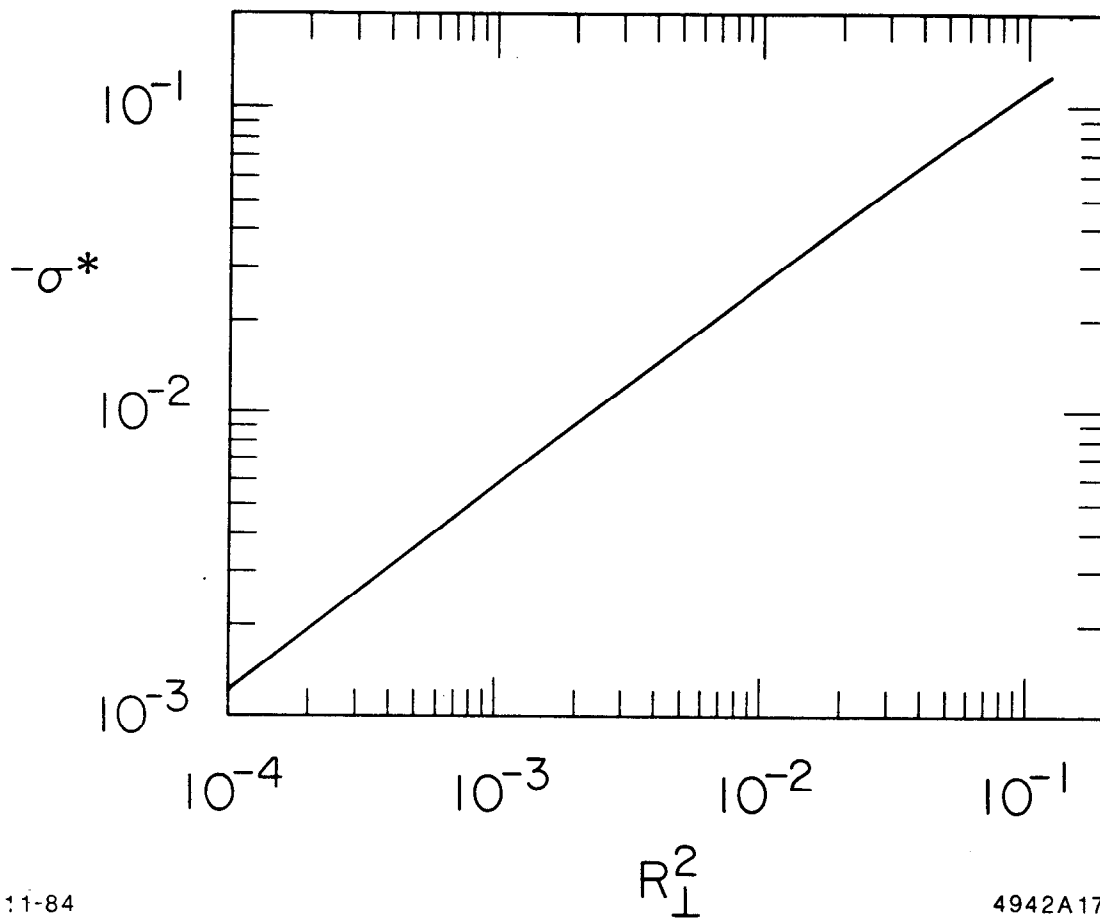
Fig. 15



11-84

4942A16

Fig. 16



11-84

R_L^2

4942A17

Fig. 17